Nanoscale

Accepted Manuscript

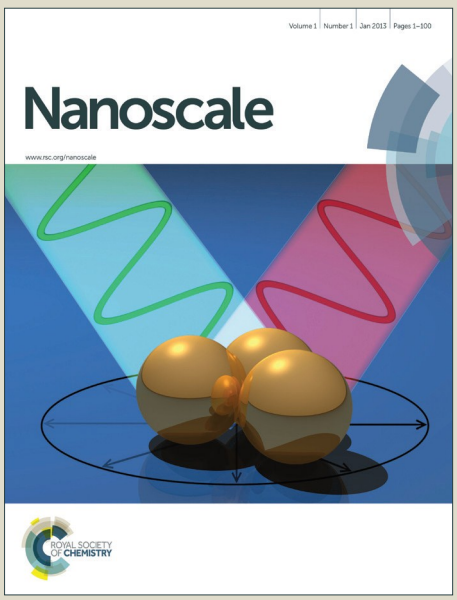




ROYAL SOCIETY OF CHEMISTRY

www.rsc.org/nanoscale

Nanoscale

REVIEW

# Syntheses and Applications of Periodic Mesoporous Organosilica Nanoparticles

Jonas G. Croissant,*[a] Xavier Cattoën,[b] Michel Wong Chi Man,[c] Jean-Olivier Durand*[c] and Niveen M. Khashab*[a]

Received 00th January 20xx,
Accepted 00th January 20xx

DOI: 10.1039/x0xx00000x

www.rsc.org/

Periodic Mesoporous Organosilica (PMO) nanomaterials are envisioned to be one of the most prolific subjects of research in next decade. Alike mesoporous silica nanoparticles (MSN), PMO nanoparticles (NPs) prepared from organo-bridged alkoxysilanes have tunable mesopores that could be utilized for many applications such as gas and molecule adsorption, catalysis, drug and gene delivery, electronics, and sensing; but unlike MSN, the diversity in chemical nature of the pore walls of such nanomaterials is theoretically unlimited. Thus, we expect that PMO NPs will receive considerable interest over the next decade. In this review, we will present a comprehensive overview of the synthetic strategies for the preparation of nanoscaled PMO materials, and then describe their applications in catalysis and nanomedicine. The remarkable assets of the PMO structure are also detailed, and insights are provided for the preparation of more complex PMO nanoplatforms.

[a.] *Smart Hybrid Materials Laboratory, Advanced Membranes and Porous Materials Center, King Abdullah University of Science and Technology, Thuwal 23955, Saudi Arabia. E-mail: niveen.khashab@kaust.edu.sa.*
[b.] *Institut Néel, Université Grenoble Alpes and CNRS, Grenoble, France.*
[c.] *Institut Charles Gerhardt Montpellier UMR-5253 CNRS-UM2-ENSCM-UM1cc 1701 Place Eugène Bataillon F-34095 Montpellier cedex 05, France.*

## 1-Introduction

### 1.1- What are PMOs?

PMO materials are obtained by the sol-gel process from organo-bridged alkoxysilanes in the presence of structure-directing

**Jonas G. Croissant**

*Dr. Jonas Croissant is a post-doctoral researcher in King Abdullah University of Science and technology (Saudi Arabia) and UCLA. He received his Ph.D. degree at the École Nationale Supérieure de Chimie de Montpellier (France) under the supervision of Prof. Jean-Olivier Durand and Michel Wong Chi Man. He was awarded the Balard Chemistry Foundation as well as the Société Chimique de France Languedoc Roussillon doctoral thesis awards. His research interests include the design and applications of organosilica nanocomposites.*

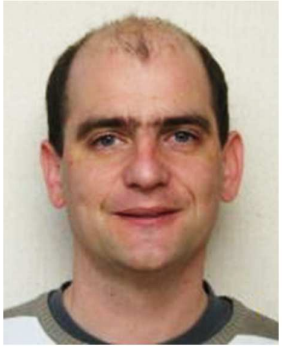

**Xavier Cattoën**

*Dr. Xavier Cattoën was born in 1978 in Poitiers (France). He graduated from ENS Cachan then completed his PhD in 2004 under the supervision of Prof. G. Bertrand and Dr D. Bourissou in Toulouse. After a post-doctoral stay at ICIQ in Tarragona (Spain) in M. A. Pericàs' group, he joined the CNRS in 2007 at ICG Montpellier, then moved to the Néel Institute, Grenoble in 2013 where he is developing structured hybrid materials for applications in biophotonics.*

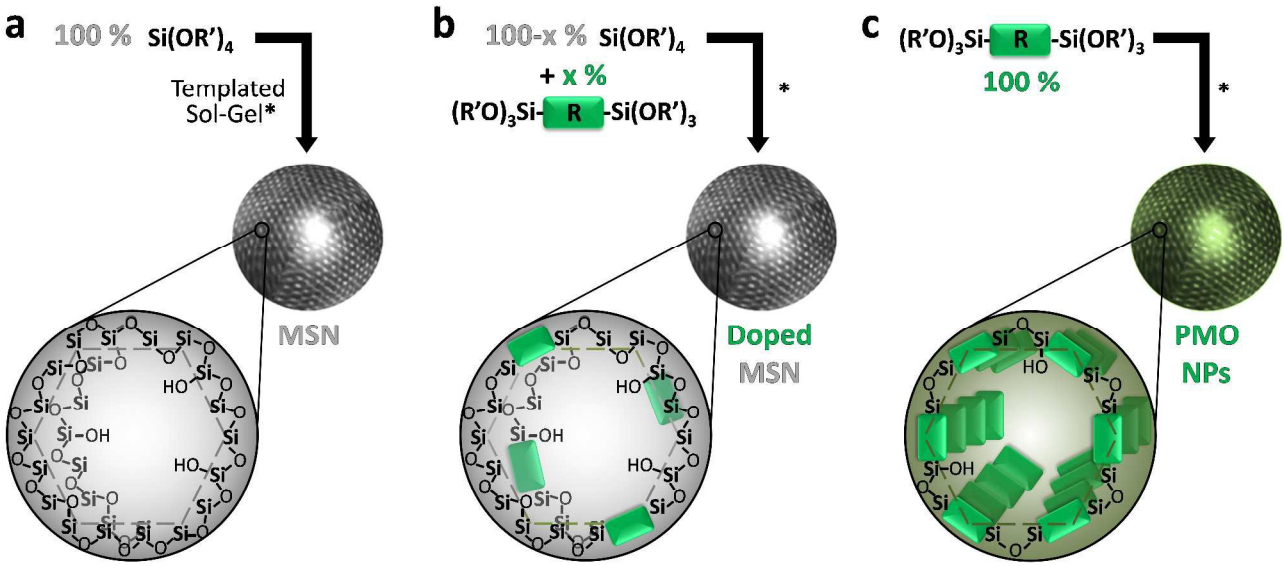


**Figure 1** Schematic representation of MSN (a), organically-doped MSN (b), and PMO NPs (c), along with their typical precursors and resulting pore functionalities. The tetravalence of silicon atoms is omitted for clarity.

agents.[1-24] Unlike MSN (see Figure 1a), the porous frameworks of PMOs are based on organic functional groups covalently linking siloxane domains.[25-38] It is noteworthy that there is a common confusion in the scientific literature between PMO materials and organically-modified mesoporous silicas (see Figure 1b-c).[39-42] We adopt here the most restrictive definition of PMOs, which should satisfy following requirements: (1) a structure based only on silsesquioxanes, which implies that the synthesis must be performed in the absence of silica source (*e.g.* tetraethoxysilane), (2) a sufficient porosity to be considered a mesoporous material, which is often a major synthetic challenge.[43-47] Among PMO materials, we may also emphasize crystal-like PMOs[4, 48] which exhibit a periodic orientation of the organic moieties within the pore walls, as phenylene[1, 27, 49, 50] and H-bonding-directed cyclohexane

**Michel Wong Chi Man**

*Dr. Michel Wong Chi Man studied at the University of Montpellier (France) before completing an AvH Postdoctoral Fellowship at the University of Heidelberg (Germany). Currently he is a CNRS Research Director working at the ICGM institute (Institut Charles Gerhardt Montpellier) and is also serving on the Board of the ISGS (International Sol-Gel Society) since 2011. He is an expert in organosilicon and hybrid silica chemistry and over the past two decades he developed pioneering work on bridged silsesquioxanes (BS) producing significant scientific advances in this field. He was the first to report right- and left-handed helical BS and self-structured BS on the nanoscale. He has also developed BS for application in several fields: catalysis, optics, separation chemistry.*

**Jean-Olivier Durand**

*Dr. Jean-Olivier Durand graduated from the Ecole Nationale Supérieure de Chimie de Paris in 1990 and obtained his PhD in organic chemistry with Prof. J. P. Genêt in 1993. He spent a 20 month postdoctoral position with Prof. W. Oppolzer at the University of Geneva (Switzerland). After two other postdoctoral studies in Rennes (Prof. Le Corre) and Paris (Dr M. Larchevêque), he was appointed a CNRS researcher in 1996 at the Laboratoire de Chimie Moléculaire et Organisation du Solide, Institut Charles Gerhardt Montpellier. His research interests include the development of mesoporous silica nanoparticles for photodynamic therapy and drug delivery.*

triamide-bridged PMO compounds;[51] whereas most PMOs contain randomly oriented organic functions.

### 1.2- The Uniqueness of PMO material

PMO materials are fundamentally unique thanks to the combination of all the advantages of a robust porous organic/inorganic framework, along with the intrinsic properties of the organic fragments.[23, 52-64] On the one hand, PMO NPs thus share the numerous assets of mesoporous silca[65-67] such as: (1) Porous channels for various applications in catalysis,[68, 69] adsorption,[70-73] drug delivery,[74, 75] light-harvesting,[21, 30, 76,] electronics,[20, 29, 77], etc. (2) Tunable pore size organization.[4, 5] (3) Engineering of the NPs outer and inner surface via the well-known silicon chemistry, thus allowing the modulation of the NPs surface functionalities and charge, as well as its dispersability in aqueous or organic solvents.[4, 70] (4) Biocompatibility, demonstrated for several types of PMO NPs.[78] On the other hand, the organic moieties of PMO materials provide: (1) Virtually unlimited applications, according to the features of the organic groups selected to constitute the pores. (2) The highest organic content in the material, thus maximizing the influence of the organic group on the overall properties of the material. Note that, having the highest organic content along with a high and accessible porosity is neither achievable with doped MSN nor with post-grafted MSN, in which case the surface area lowers significantly after grafting. (3) The modulation of the hydrophilicity/hydrophobicity of the pores, which permitted for instance much higher drug loading capacities.[2, 79, 80] (4) Additional features arising from crystal-like PMO materials, such as molecular rotors with phenylene[81] and fluorinated p-divinylphenylene bridges, the latter also displaying a dielectric response.[50] (5) The PMOs may be degraded under certain conditions when specific functional groups sensitive to acid-basic, redox, photochemical, or biochemical reactions are present in the structure of the organic framework.[2, 82] (6) Post-modification of the organic fragment by classical organic chemistry.[4, 83, 84]

**Niveen M. Khashab**

*Dr. Niveen M. Khashab received her BSc degree from the American University of Beirut in 2002 and her PhD degree from the University of Florida, Gainesville in 2006 with Alan Katritzky. She conducted postdoctoral studies with Sir J. Fraser Stoddart in UCLA and Northwestern from 2007 to 2009. She joined King Abdullah University for Science and Technology in June 2009 as an Assistant professor. Her major interests include hybrid materials, stimuli responsive systems, controlled release and delivery applications, and self-assembly.*

### 1.3- Pioneering Works

In the year 1999, the research groups of Inagaki, Ozin, and Stein independently described the first PMO materials.[85-87] Inagaki and coworkers produced and investigated ethylene-bridged ($-CH_2-CH_2-$) PMO bulk material using the octadecyltrimethylammonium surfactant. Structures with 2D and 3D hexagonal pore arrays of 2.7 and 3.1 nm were obtained depending on the surfactant concentration. Ozin *et al.* prepared ethylene-bridged PMO from CTAB,[86] while Stein *et al.* synthesized both ethylene- and ethenylene-bridged (-CH=CH-) PMOs with the first post-synthetic modification of the organic groups, turning ethenylene moieties into dibromo-ethylene ones.[87] Besides, the group of Inagaki reported in 2002 a crystal-like architecture in a phenylene-bridged ($-C_6H_4-$) PMO material, as described in the molecular simulation in Figure 2.[49] In 2010, the acronym "PMO" was coined by Ozin *et al*., and the functionalities of these materials were reviewed.[88]

Since then, many groups have developed versatile bulk PMO materials from bridged organoalkoxysilane with organic fragments such as butylene ($-CH_2-CH_2-CH_2-CH_2-$),

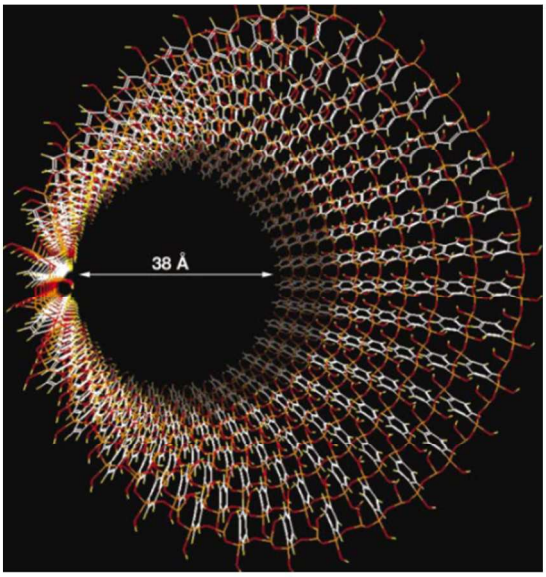


**Figure 2** Molecular simulation of the phenylene-bridged PMO pores. Copyright 2002, Nature Publishing Group.[44]

biphenylylene ($-C_6H_4-C_6H_4-$), thiophene ($-C_4H_2S-$), bithiophene ($-C_4H_2S-C_4H_2S-$), bipyridine ($-C_5H_3N-C_5H_3N-$), etc, and we refer readers to excellent reviews that have been published on the subject.[4, 89, 90] Notably, PMOs were also reported as micron-size powders from organo-bridged alkoxysilanes with complex organic fragments: dendrimers,[11] perylene bisimide,[20] as well as in thin films (though TEOS was needed) via polyhedral oligomeric silsesquioxane blocks,[91] prophyrins,[92] and zinc phthalocyanine.[93]

## 2- REACHING THE NANOSCALE

Although a wide variety of bulk PMO materials has been reported, reaching the nanoscale for such material is much more challenging and has been less studied. In this section, the main soft and hard templating synthetic pathways for the construction of PMO NPs will respectively be classified by their morphology and template type, and discussed in chronological order. An aerosol-assisted approach will also be presented.

### 2.1- Soft templating strategies

**Spherical NPs.** In 2006, the first PMO NPs were reported with a hollow spherical morphology, thanks to the use of the FC-4 fluorocarbon surfactant [$C_3F_7O(CFCF_3CF_2O)_2$-$CFCF_3CONH(CH_2)_3$-$N^+(C_2H_5)_2CH_3$, $I^-$] and the cetyltrimethyl-ammonium bromide (CTAB) cationic surfactant as co-structure directing agents. Ethylene-bridged hollow PMO (HPMO) NPs were prepared from 1,2-bis(trimethoxysilyl)ethane (see Figure 3),[94] with sodium hydroxide catalysed sol-gel reaction at 80°C. This approach led for the first time to PMO nanomaterials, with sizes ranging from 100 to 400 nm in diameter. Moreover, by varying the FC-4 over CTAB ratio the shell thickness of the HPMO NPs could be tuned, while non-hollow PMO microspheres were obtained by using only the CTAB surfactant. Later on, hydrophobic iron oxide ($Fe_3O_4$) NPs and silica-covered barium ferrite ($BaFe_{12}O_{19}$) NPs could be embedded within HPMO NPs after CTAB stabilization before the formation of the FC-4 vesicles.[95, 96] Furthermore, functional, mixed HPMO NPs could be obtained by co-condensation of the ethane precursor with propyltriethoxysilanes ($X-(CH_2)_3-Si(OEt)_3$, with X = SH, $NH_2$, C≡N, C=CH, $C_6H_5$).[97]

Phenylene-bridged PMO nanospheres were then reported in 2009, with a diameters ranging from 50 to 1000 nm, and a worm-like porosity.[98] The procedure was based on a co-templating by a poly(ethylene oxide)-poly(DL-lactic acid-co-glycolic acid)-poly(ethylene oxide) triblock copolymer and the FC-4 surfactant in water/ethanol under acidic conditions. Interestingly, a core-shell structure with a porous core and a thin, less porous shell was observed, which suggests that both surfactants were immiscible, the shell being templated by FC-4 and the core by the poly-lactic acid based polymer. Using the well-known P123 block co-polymer, but without FC-4, ethylene- or phenylene-bridged hollow organosilica nanospheres of 12 to 25 nm were obtained, instead of the expected PMO materials.[99] The size and textural properties of these materials could be easily tuned by adding trimethylbenzene. In 2011, colloidal solutions of monodisperse PMO nanospheres of 20 nm in diameter were reported, for simple organic bridges such as methylene, ethylene and ethenylene, but not for the larger phenylene linker.[100] These nanoparticles, which feature a worm-like porosity, were obtained from a basic aqueous mixture of CTAB and triethanolamine at 80ºC for 6 h, followed by dialysis.

Until that point, PMO NPs were limited in the organic group constituting the pore walls, the size, and the monodispersity of the nanomaterials. In 2012 a remarkable

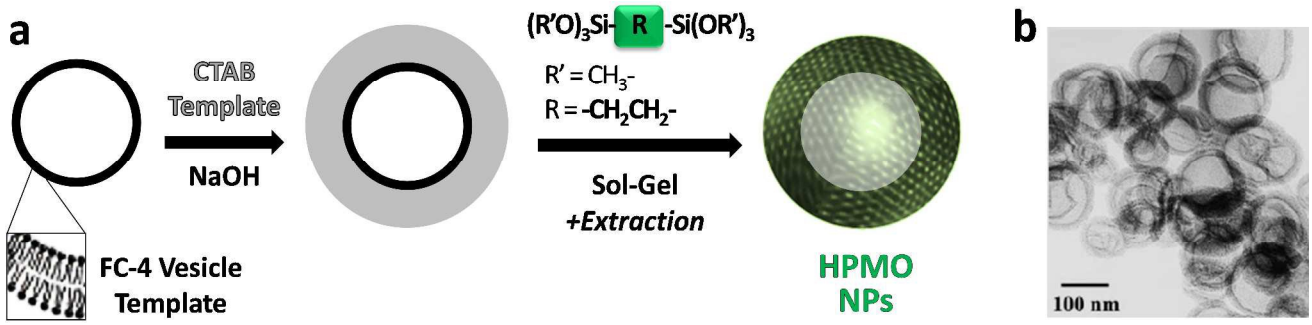


**Figure 3** Schematic representation of the FC-4 vesicle and CTAB dual templating strategy for the preparation of HPMO NPs (a), and a Transmission Electron Microscopy (TEM) image of a resulting nanomaterial (b). Micrograph reproduced with permission, copyright 2006, American Chemical Society.[94]

synthetic process was reported for the preparation of monodisperse methylene-, ethylene-, ethenylene-, and phenylene-bridged PMO NPs with highly ordered pore structures and typical NPs diameters of 100 to 200 nm (Figure 4).[101] These NPs were produced using CTAB as structure-directing agent at 50°C for 6 h with ammonia as catalyst.

**Nanorods and nanofibers.** Jaroniec *et al*. first described in 2008 the controlled synthesis of ethylene-phenylene 200 nm wide microrods with coil-like morphology.[102] In 2009, using the trisilylated octaethoxy-1,3,5-trisilapentane precursor, among different nano-objects PMO nanorods (700 × 200 $nm^2$) and nanofibers (100 × 2000 $nm^2$) were obtained with adjustable aspect ratio from 2:1 to 20:1 by varying the concentration of the precursor.[103, 104] They also obtained PMO nanofibers of 100 nm in diameter and tens of microns in length at low precursor concentration, and one-dimensional nanostructures were not observed for tetraethoxysilane or bis(triethoxysilyl)-methane.[104] The use of the pluronic P123 triblock copolymer structure-directing agent under acidic conditions resulted in an average pore diameter of 4.3 nm. Later on, methylene-, ethenylene, and phenylene-bridged PMO helical fibers were reported using CTAB and (S)-β-citronellol as templating agents.[105] The fibers were100 to 300 nm wide and up to micron length, however their sizes could be tuned to obtain nanorods depending on the precursor used.

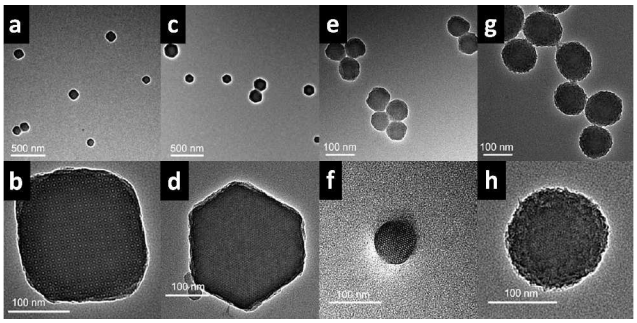


**Figure 4** TEM images of ethylene- (a,b), methylene- (c,d), ethenylene- (e,f), and phenylene-bridged PMO NPs (g,h) at low and high magnifications. Reproduced with permission of the Royal Society of Chemistry.[101]

PMO rods (70–150 × 1000–5000 nm) with clickable functions were obtained by the hydrolysis-condensation of precursors of the general formula $(EtO)_3Si-(CH_2)_3-NR-(CH_2)_3-Si(OEt)_3$ with R = $-CH_2-C{\equiv}CH$; $-(CH_2)_2-N_3$; $-(CH_2)_3-N_3$, using cetyl stearyl sulfate (SHS) in acidic medium.[83] Though these rods were quantitatively functionalized by the so-called CuAAC click reaction, their 2D-hexagonal mesostructure collapsed upon outgassing. Monodisperse ethenylene-bridged PMO nanorods (450±100 × 200±50 $nm^2$) were also prepared using CTAB in basic aqueous solution. Moreover, mixed PMO NPs were obtained from the co-condensation of bis(triethoxysilyl)ethane (E) with bis(3-triethoxysilylpropyl)-disulfide) (DIS), leading to porous nanorods with various aspect ratios, whereas the hydrolysis-condensation of DIS alone yielded dense nanospheres (see Figure 5). The resulting mixed PMO NPs displayed highly ordered 2 nm pores. Furthermore, the good mixing of the two precursors resulted in an efficient degradation upon disulfide cleavage by mercaptans.[2]

**Nanotubes.** Though nanotubes cannot really be considered as PMOs as no organized porosity is present in the walls, these

nanoscaled, highly porous bridged silsesquioxanes deserve surfactant.[108] Interestingly, the absence of spatial segregation particular attention. Using P123 in acidic medium, ethylene- between the phenylene and bipyridine moieties was evidenced and phenylene-bridged organosilicas could be produced on by electron microscopies.
large scale as nanotubes (100 to 600 nm long, with 6 nm of
inner diameter and thickness of 3 nm).[106] This enabled the **Metal or metal oxide core PMO shell NPs.** $Co_3O_4$ core generation of palladium NPs within the nanotubes via ethenylene-bridged PMO shell nanospheres were also impregnation of palladium dichloride and subsequent developed through CTAB micellar stabilization of the cobalt reduction. Interestingly, ethylene-bridged organosilica oxide cores.[109] The resulting NPs were of 130 nm with a nanotubes generated bigger Pd NPs (4.8 nm) than the benzene spherical morphology and had 240 to 480 $m^2/g$ of surface area. ones (1.8 nm). In 2012, the transition of ethylene-bridged This platform was studied for as model for biocatalytic organosilica hollow nanospheres to nanotubes was studied processes. In parallel with the design of ethenylene- and through adjustment of the surfactant.[107] Indeed, P123 is known phenylene-bridged PMO NPs, we recently described a versatile to afford easily cylindrical micelles, and led to nanospheres, strategy for the preparation of core-shell PMO NPs through a whereas F127, which features a higher hydrophilicity, led to soft templating method.[110] Our aim was to incorporate within hollow nanospheres. Finally, mixed phenylene-bipyridine- an organized PMO framework a bulky organic fragment bridged organosilica nanotubes with 7.8 nm inner diameter containing four
were obtained by the co-condensation method using the P123

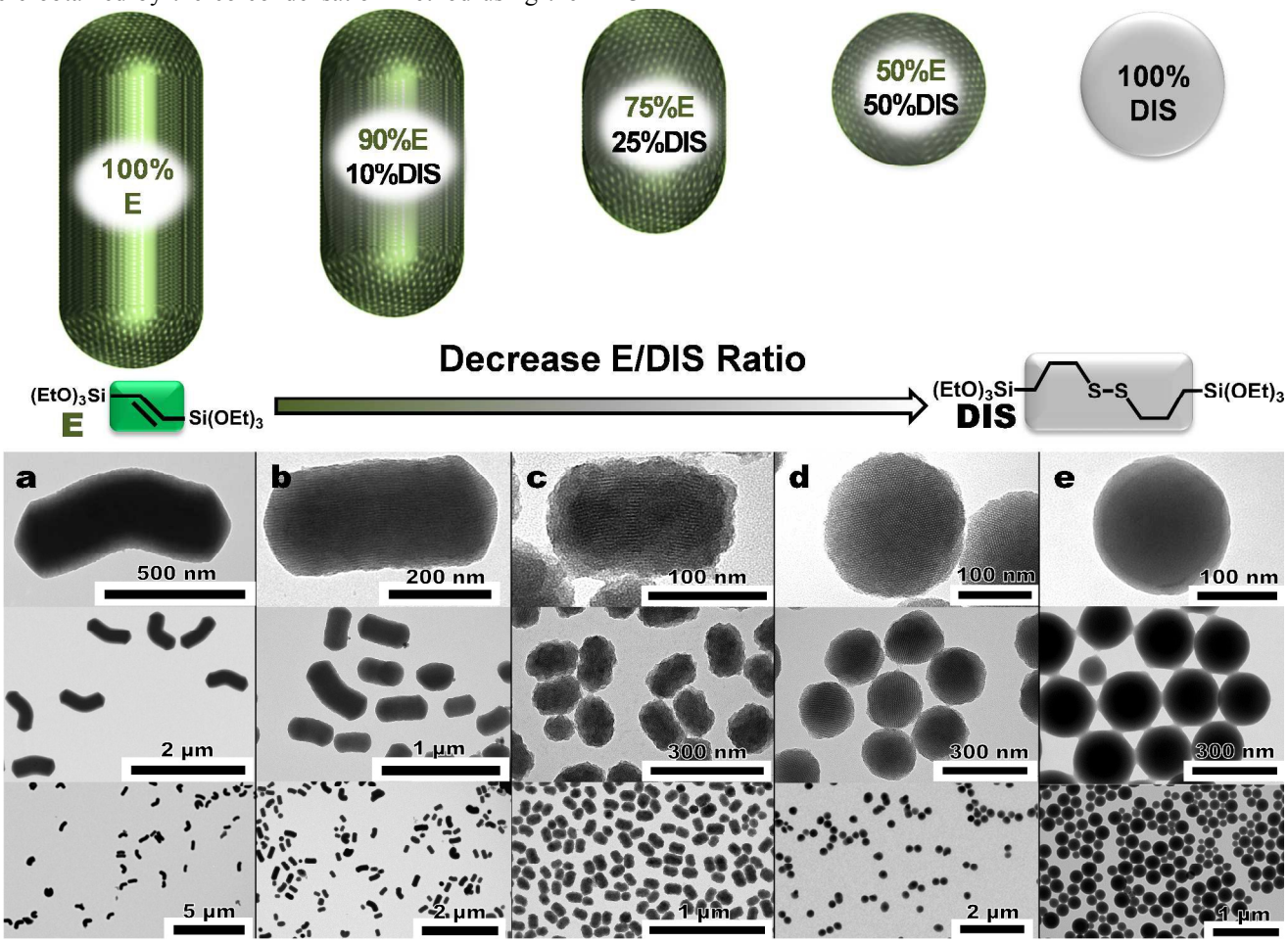


**Figure 5** Schematic representation of the size and morphology control in ethenylene-bridged PMO (a), ethenylene-bis(propyl)disulfide-bridged PMO (b-d), and bis(propyl)disulfide non-porous bridged silsesquioxane NPs (e) by the variation of the E/DIS precursor ratio in the reaction media. TEM images of NPs obtained from E/DIS ratios of 100/0, 90/10, 75/25, 50/50, and 0/100 (a-e respectively). Adapted with permission, copyright 2014, Wiley.[2]

trialkoxysilyl groups, which acted as a two-photon photosensitizer (see "2PS" precursors in Figure 6).[111] Hence we decided to co-condense the ethenylene (E) or the phenylene (B)-based precursors with 2PS molecules and we obtained two-photon-sensitive E2 or B2 mixed PMO NPs respectively (see Figure 6a). Then, according to a modified one-pot synthesis of gold core mesoporous silica shell in an aqueous CTAB template,[112] we constructed gold core ethenylene- or phenylene-bridged PMO shell NPs (AE and AB NPs respectively, Figure 6b). Moreover, by co-condensing the 2PS with E or B precursors along with the in-situ generation of gold nanocrystals we could also respectively obtain the two-photon-sensitive AE2 and AB2 core-shell NPs (Figure 6c).

**Multipodal NPs.** We also recently designed unique multipodal PMO NPs with phenylene-bridged cores and ethenylene-bridged pods prepared in a one-pot two-steps process via NaOH catalysis in CTAB-templated aqueous media. While the sole condensation of 1,4-bis(triethoxysilyl)benzene or 1,2-bis(triethoxysilyl)-ethylene precursor, respectively produced phenylene- and ethenylene-bridged PMO nanospheres and nanorods (Figure 7a and b), the subsequent addition of the ethenylene precursor in a solution of freshly-prepared phenylene-bridged NPs generated multipodal nano-objects (Figure 7c). Note that, the reverse addition of 1,2-bis(triethoxysilyl)ethylene followed by bis(triethoxysilyl)-benzene produced phase-segregated nanomaterials. In the multipodal NPs, phenylene-bridged cores were of spherical morphology with diameters of 130±20 nm and displayed a radial porosity. Besides, a crystal-like architecture within the pores walls was clearly deduced from the X-ray

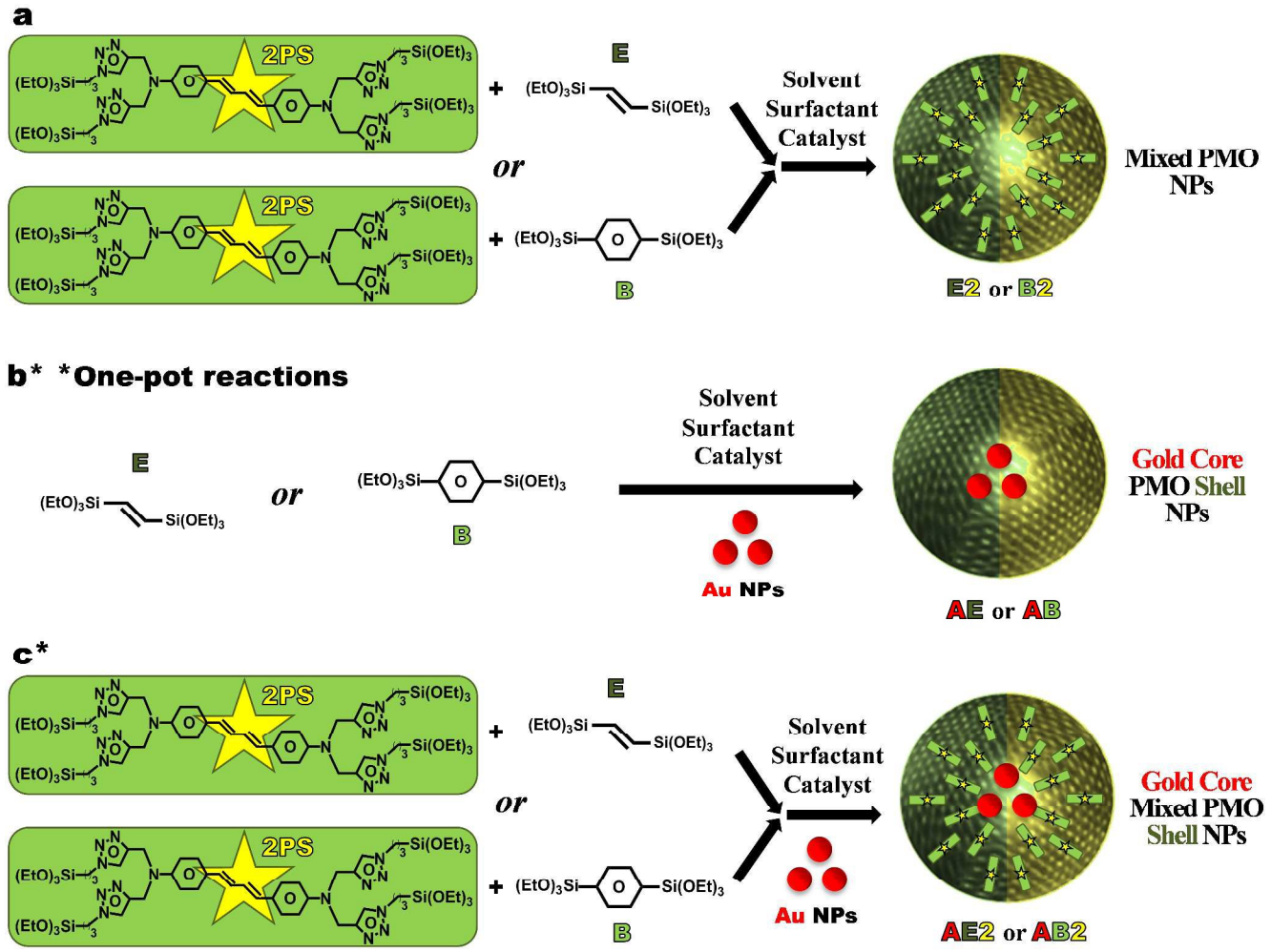


**Figure 6** Design of E2 or B2 Mixed PMO NPs, obtained from the 2PS and either bis(triethoxysilyl)ethylene (E), or bis(triethoxysilyl)benzene (B), respectively (a). One-pot synthesis of AE or AB gold core PMO shell NPs, respectively composed of either the E or the B moieties (b). One-pot synthesis of AE2 or AB2 gold core Mixed PMO shell NPs, composed of either 2PS and E (AE2), or 2PS and B (AB2) (c). Adapted with permission, copyright 2014, American Chemical Society.[110]

diffractograms.[1] Ethenylene-bridged PMO pods were 100-150 nm long and 100 nm in diameter, and displayed 2-D hexagonal periodic structure with very high surface areas and pore volumes in the order of 1500 $m^2/g$ and 1.2 $cm^3/g$. Recently D. Zhao's group reported Janus NPs which were constituted of up-conversion core MSN shell onto which ethenylene-bridged cubic pods grew.[113] Such NPs were used for dual cargo delivery via temperature and light triggers.

### 2.2- Hard templating strategies

As an alternative to the soft templates such as FC-4 vesicles to form hollow PMO spheres, the use of hard templates such as silica or metal oxide has emerged. The synthesis of these NPs with controlled sizes is well mastered. Furthermore the differential reactivity towards acids or bases allows etching the core template without degrading the PMO shell.

**Silica sphere template**. Dense silica NPs can be easily prepared by the Stöber method or using reverse microemulsions, with narrow size distribution. Typically, dense silica spheres are first prepared, then PMO shells are grown on such NPs (Figure 8a-b). Finally, the silica core is partially or fully degraded in order to obtain PMO nanorattles or HPMO NPs, respectively (Figure 8c and d). Such a strategy was reported for the first time in 2010[114] for the formation of core-shell nano-objects with dense silica cores of 400 nm in diameter, surrounded by 75 nm thick phenylene-bridged PMO shells. The PMO synthesis was performed using CTAB under basic catalysis. Interestingly, raising the temperature of the

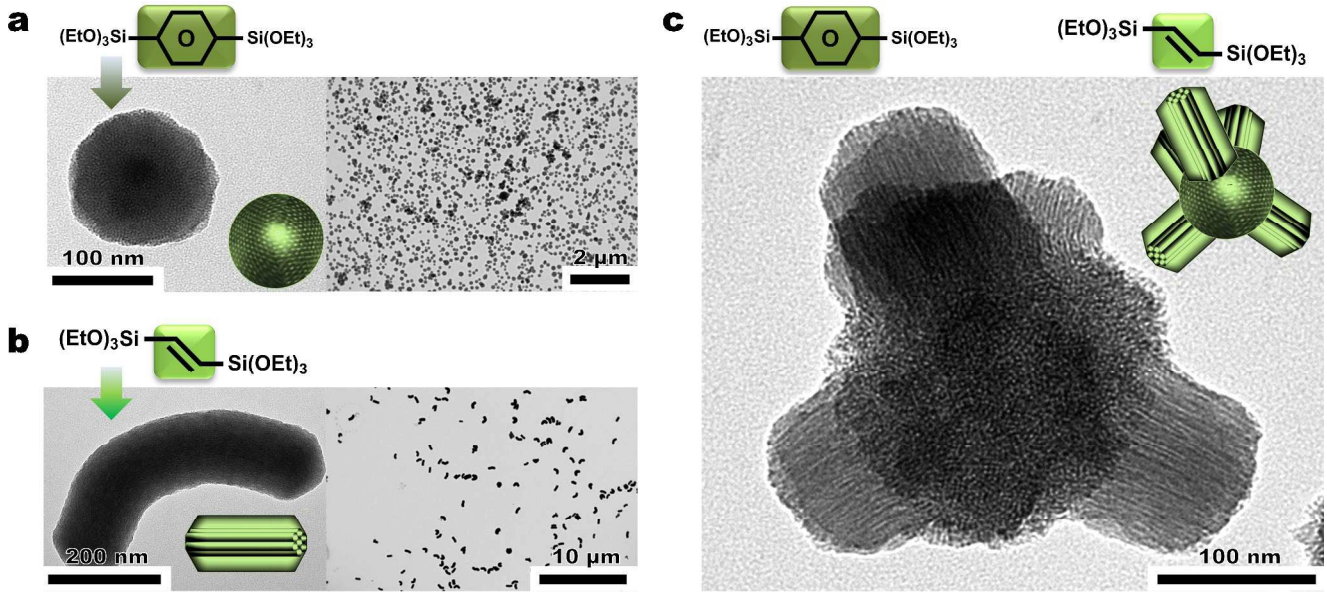


**Figure 7** TEM images of phenylene-bridged PMO nanospheres (a) and E PMO nanorods (b) obtained solely from the bis(triethoxysilyl)benzene or bis(triethoxysilyl)ethylene precursors. TEM micrograph of a multipodal phenylene-ethenylene-bridged PMO NP designed from a one-pot two steps condensation process. Adapted with permission, copyright 2014, Wiley.[1]

shell synthesis from 25 to 100°C induced a shrinkage or partial dissolution of the core, which led to 'nanorattles', or yolk-shell NPs.

Another strategy to form such $SiO_2$@PMO nanorattles consists in surrounding dense silica NPs with a FC-4 vesicle, then condensing ethane-silica around it. After extraction, yolk-shell NPs (*ca* 200 nm), with perpendicularly aligned mesopores and tunable void (4 to 52 nm) and shell thickness (16 to 34 nm) were obtained. Interestingly, metal NPs such as gold, platinum, and palladium could be formed in the void space between the core and the shell using impregnation and reduction of specific metal precursors (see Figure 9).[115] The complete dissolution of the silica cores in $SiO_2$@ethylene-bridged organosilica was achieved in 2013, with the formation of 50 nm porous organosilica hollow-spheres upon selective dissolution with sodium hydroxide at pH 13.[116] During the same year, various HPMO NPs with ethylene, ethenylene, and phenylene organic linkers (see phenylene-bridged NPs in Figure 8c-d) were obtained by dissolution of silica from larger $SiO_2$@PMO core-shell NPs.[3] Depending on the dissolution protocol used, nanorattles (using hydrofluoric acid) or HPMO NPs (using sodium carbonate) could be obtained. Mixed HPMOs incorporating up to five different, miscible bridged organoalkoxysilanes (R = $-CH_2-CH_2-$, $-CH=CH-$, $-C_6H_4-$, $C_6H_4-C_6H_4-$, $-(CH_2)_3-S_4-(CH_2)_3-$) were

prepared through the same strategy.[78] Notably, TEM imaging showed a homogeneous dispersion of the sulfur atoms throughout the structure.

Core-shell iron oxide-MSN ($Fe_3O_4$@MSN) and Au@MSN nanoparticles were also used as hard templates for the preparation of $Fe_3O_4$@HPMO and Au@HPMO nanorattles. Mechanistic investigations showed that the formation of the PMO shell occurred concomitantly with the dissolution of the MSN core within minutes. However, the silicon environments were equally distributed between T (C-$SiO_3$) and Q environments ($SiO_4$), which means that the silicates were partially redistributed and co-condensed with the organosilica.[117] Nonetheless, the aforementioned NPs, of a hundred nanometer in diameter, were aggregated in the micron range.

**Iron oxide sphere template.** Another hard templating strategy involves the use of hematite ($Fe_2O_3$) NPs. Phenylene-bridged HPMO NPs, incorporating clickable azidopropyl groups were prepared by condensation of BTEB around hematite NPs with CTAB under basic conditions for 2 h at 80°C. Surfactant removal and etching were performed in two steps using hydrochloric acid (see Figure 11 in the catalysis section).[118]

**Polystyrene template.** A very simple strategy to prepare large HPMO NPs (350 nm) involves the use of polystyrene beads, which are available with very low size dispersity. This template is easily removed by THF extractions.[119]

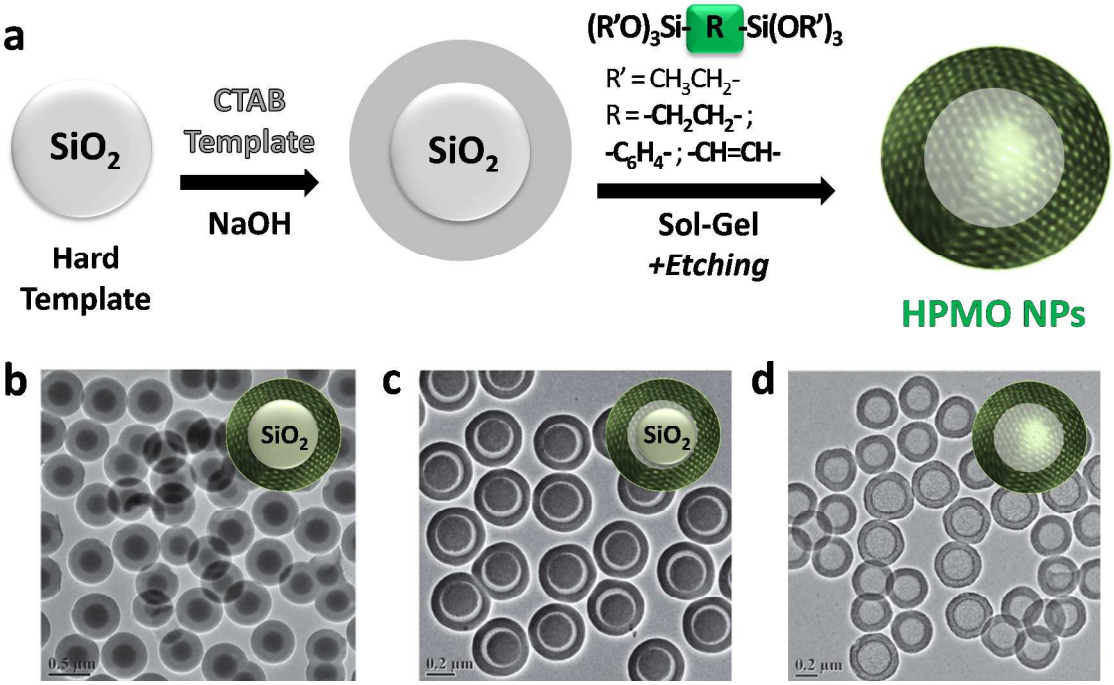


**Figure 8** Schematic representation of the silica spheres hard templating strategy for the design of HPMO NPs (a). TEM images of $SiO_2$@HPMO NPs before etching (b), $SiO_2$@HPMO nanorattles after partial etching (c), and HPMO NPs after complete etching (d). Micrographs reproduced with permission, copyright 2014, Wiley.[3]

Comparing soft and hard templating strategies, we may generally conclude that: (1) soft templating methods are more simple and faster since they do not require the preparation and removal of a hard template. (2) Both soft and hard templating strategies could be used to design HPMO NPs. However, hard templating strategies often (though not always) provide more monodisperse and controlled NPs, but, the size of the resulting HPMO is generally (though not necessarily) higher than 200 nm, which is not ideal for biomedical applications. (3) Hard templating strategies enable the preparation of silica@HPMO nanorattles, as well as the presence of metal and metal oxide NPs within HPMO NPs, which is of particular interest for catalysis as we shall see in the application section. (4) To date only soft templating approaches produced the long range molecular periodicity of organic fragments, required for specific properties and applications of PMOs.

### 2.3- Aerosol-assisted strategy

An original approach consisting in an aerosol-assisted nanomaterial synthesis was first described in 1999 by Brinker

*et al.* for MSN,[120] and PMO NPs with phenylene and butylene bridging groups in 2000.[121] The recent work of Sebastian Polarz *et al.*[122] illustrates the principle of this technique (see Figure 10a) which consists in the continual nurrishing of an aerosol

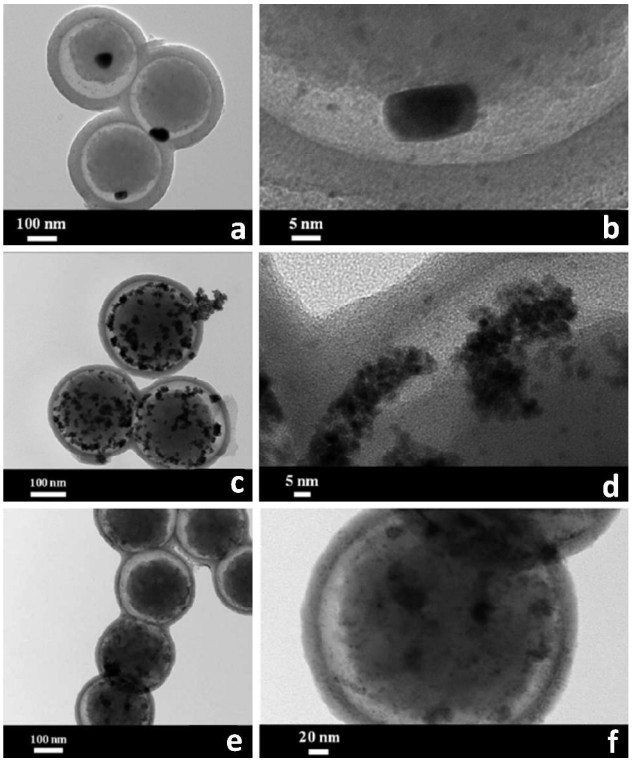


**Figure 9** TEM and High-Resolution TEM images of ethylene-bridged PMO nanorattles with $SiO_2$@Au (a,b), $SiO_2$@Pt (c,d), and $SiO_2$@Pd cores (e,f). Reproduced with permission, copyright 2012, Wiley.[115]

generator from an aged sol containing a non-ionic copolymer (typically pluronic F127 or P123) an organo-bridged alkoxysilane, water and ethanol in acidic conditions. The mixture is then nebulized as droplets and dried through a tube oven which leads to polydisperse, non-aggregated PMO nanospheres of 100 to 1000 nm in diameter (Figure 10b). PMO NPs based on Br-, $CO_2H$-, $NH_2$-, and $SO_3H$- ortho-functionalized phenylene groups (see Figure 9a), with worm-like porosity and variable surface areas (270-720 $m^2/g$) can be obtained on large scale by this method. Besides, PMO NPs containing $SO_3H$ groups possessed super acidic properties and were applied for antifouling applications.[122] They also reported thiol ortho-functionalized phenylene-bridged

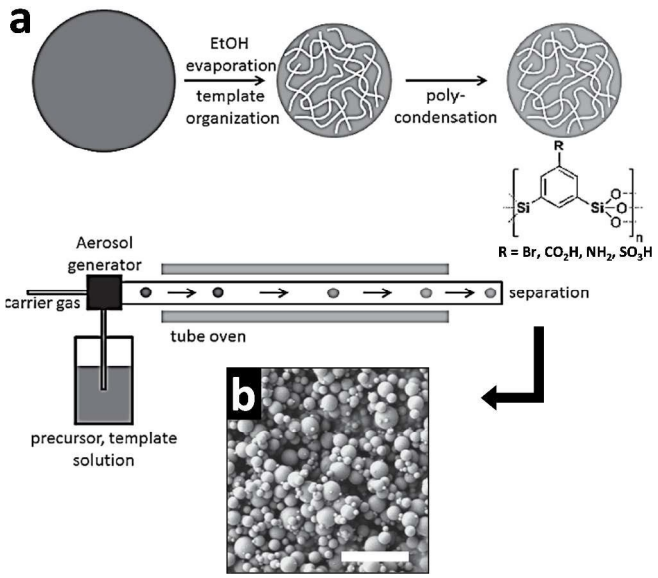


**Figure 10** Schematic representation of the setup used for the preparation of PMO NPs via the aerosol-assisted process (a), and scanning electron micrograph of the resulting NPs (b). Scale bar of 2 µm. Adapted with permission, copyright 2014, Wiley.[122]

PMO nanospheres which they encapsulated and covered with silver nanoparticles for antibacterial activity.[123] PMO NPs obtained via aerosol were also designed with ethylene bridging groups though with low surface area (140 $m^2/g$).[124] It is noteworthy that this technique generally leads to limited surface areas (for such NPs) in the order of 400-500 $m^2/g$, due to non accessible pores.

## 3- APPLICATIONS OF PMO NPs

Thanks to the rich chemistry available in the pores of PMO nanomaterials, various applications have been carried out in the past few years such as carbon dioxide capture,[125] lithium ion batteries,[126] and cell adhesion with PMO NPs-hydrogel to name a few.[127] Here, we will briefly describe all the studies reported in catalysis and nanomedicine.

### 3.1- PMO NPs in Catalysis

PMO materials are increasingly studied to catalyze organic reactions.[128, 129] However, nanosized catalyst are more efficient than bulk catalyst for four main reasons: (1) The smaller the catalyst material is, the higher the outer surface area to volume ratio, thus producing higher catalytic efficacies, (2) the smaller a porous material is, the smaller diffusion pathways for reactants and products, (3) PMO NPs can possess a hollow structure to become nanoreactors.

Various types of catalysts can be supported on PMOs, such as metallic salts, metal NPs, or organocatalysts, for acid/base catalysis, oxidation and reduction, or carbon-carbon bond forming reactions.

**Organocatalysis on PMOs.** In a first example, 20 nm acidic HPMO spheres consisting of ethenylene-bridged silsesquioxanes and sulfonic acid groups have been used to support enantiomerically pure *trans N,N'* dipropylcyclohexane-1,2-diamine through electrostatic interactions with 91% yield and enantiomeric excess (*ee*) of 96%.[130] Excellent activities and stereoselectivities were obtained for the solvent-free aldol reaction between cyclohexanone and 4-nitrobenzaldehyde thanks to a dual activation, the amine groups enabling the formation of nucleophilic enamines by reaction with the ketone, and the acidic groups promoting the electrophilic activation of the aldehyde. Unfortunately, the catalytic activity strongly decreased upon recycling, though no sign of catalyst leaching could be evidenced. A MacMillan catalyst could also be anchored on 100-200 nm phenylene-bridged HPMO NPs using the CuAAC click reaction (see path B Figure 11).[118] Excellent catalytic activities were reported for the Diels-Alder reaction of cinnamaldehyde with cyclopentadiene in water (see Table 1), with a good reusability (up to 7 runs), but slightly lower enantioselectivities than the homogeneous catalyst. Moreover, the superior activity of the hollow PMO NPs compared to the analogous full PMO NPs was evidenced, as well as the improved catalytic activities and enantioselectivities with materials obtained by click grafting *vs* the ones formed by conventional grafting, which is related with a more regular spatial distribution of the organic catalytic fragments.

**Table 1** Comparison of catalytic performances of the homogeneous and supported MacMillan catalysts.

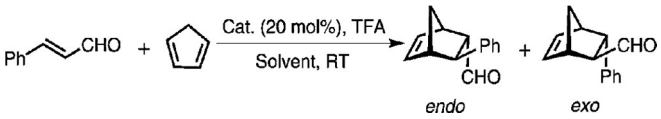


| Compound | Yield (%) | *endo ee* (%) | *exo ee* (%) |
|---|---|---|---|
| Homogenous Catalyst | 80 | 93 | 91 |
| HPMO-Mac NPs | 98 | 81 | 81 |
| PMO-Mac NPs | 84 | 79 | 78 |

**Metal NPs-supported on PMO nanoreactors.** The formation of methyl isobutyl ketone (MIBK) from acetone and dihydrogen on hollow nanospheres composed either of silica or of ethylene-bridged PMO functionalized with sulfonic acid fragments and Pd NPs was investigated.[131] This reaction proceeds in two steps, the first one involving an aldolization-crotonization reaction yielding methyl isobutylene ketone, which is then catalytically reduced by hydrogen on Pd NPs. One of the challenges for this reaction is to control the extent of by-products formation resulting from further aldol reactions. Though the organosilica nanospheres gave good conversions and selectivities, better results were obtained with the analogous sulfonic acid-silica hollow nanospheres.[130] These results were corroborated by water and acetone sorption experiments, which showed a higher hydrophilicity and affinity towards acetone for the silica NPs with respect to PMO NPs. This study confirms that a fine tuning of the PMO surface properties should enable improved catalytic properties. The hydrogenation reaction was also studied on Pd NPs forms within organosilica nanotubes.[106] Ethylene- and phenylene-bridged organosilica nanotubes of similar diameter induced very different Pd NP sizes (4.8 nm for E vs 1.8 nm for B), as a result of a strong NP stabilization by the phenylene groups. This promoted a faster catalytic reduction of cyclohexene by hydrogen for phenylene-bridged nanotubes.

Palladium NPs formed within the voids of $SiO_2$@PMO nanorattles (Figure 9e-f) were used for the oxidation of various benzylic and allylic alcohols using molecular oxygen (see Table 2).[115] Interestingly, a full selectivity towards the aldehydes was observed.

Au@HPMO yolk-shell structures are also very interesting in catalysis. This type of NPs has been applied for the selective reduction of nitroarenes, such as 2-nitroaniline[117] or 4-aminophenol with sodium borohydride.[132] Yang and co-workers however reported that a single gold NPs anchored inside a porous shell of HPMO NPs was better than Au@HPMO nanorattles, showing higher catalytic efficiency for 4-nitrophenol reduction.[133]

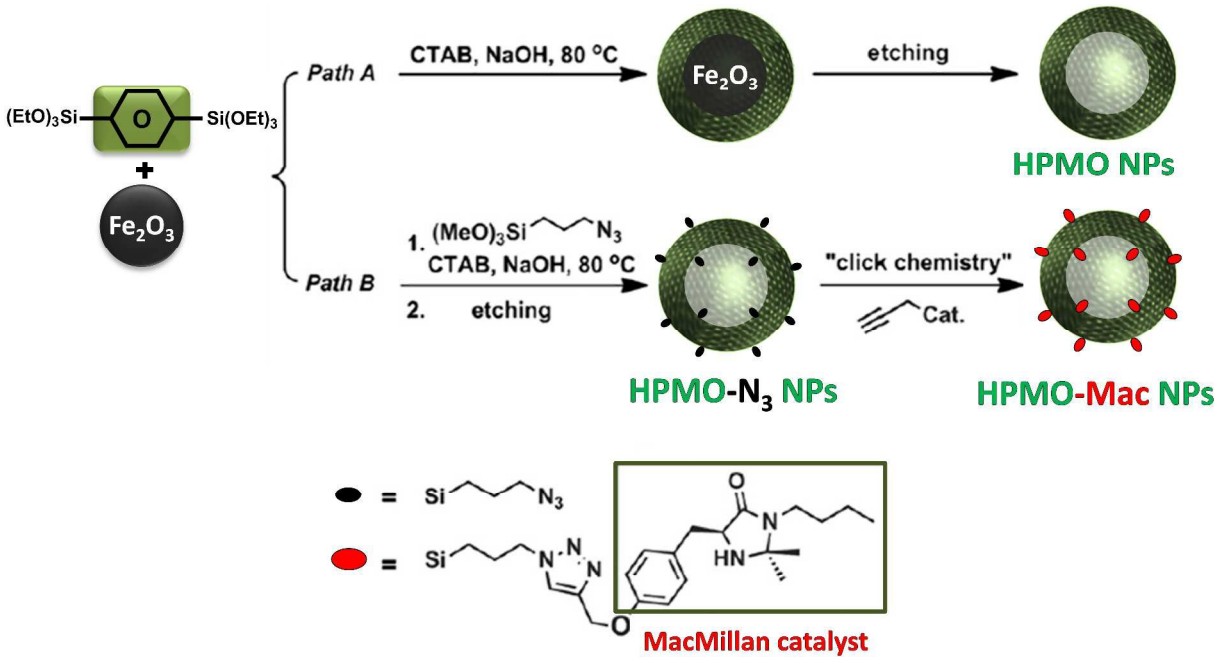


**Figure 11** Schematic representation of hard template preparation of phenylene-bridged HPMO NPs (path A), and their clickable equivalent (path B), for the MacMillan catalyst covalent post-grafting. Adapted with permission, copyright 2011, Wiley.[118]

**Table 2** Selective oxidation of various alcohols into aldehydes via ethylene-bridged HPMO nanorattles with $SiO_2$@Pd cores.

| | Reagent | Yield | Product |
|---|---|---|---|
| 1 | 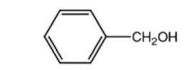 | 94 % | 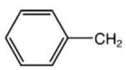 |
| 2 | 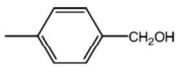 | 92 % | 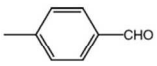 |
| 3 |  | 100 % | 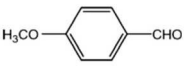 |
| 4 | 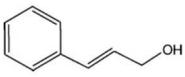 | 100 % | 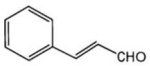 |
| 5 | 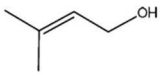 | 53 % | 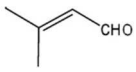 |

**Metal complexes-supported on PMO nanoreactors.** A very interesting feature of PMO materials is the virtually infinite possible variations of the organic bridging group of the structure. Whereas most studies have dealt with benzene- or ethane-silica co-condensed with a catalytic precursor, Inagaki *et al* very recently managed to prepare large PMO NPs (300-500 nm) based only on the 2,2'-bipyridine fragment.[134] The bipyridine ligand is able to strongly bind to a wide variety of transition metals (Ru, Ir, Re, Pd…), which enables its application for many catalytic reactions. High metal loading capacities were demonstrated, in particular for Re(I) and Pd(II) (1.12 and 0.74 mmol $g^{-1}$, respectively). Theses PMO NPs were tested as ligands in the catalytic borylation of arenes by Ir(I), and also proved to be efficient for the photocatalytic hydrogen formation from water. For this transformation, $Ru(bpy)_2$(BPy-PMO) complexes and Pt NPs were formed within the pores, the Ru PMO acting as photosensitizer while the Pt catalyzed the water reduction. Bipyridine ligands were also incorporated within phenylene-bridged organosilica nanotubes. Once complexed with the Cp*IrCl fragments, these NPs were used for the oxidation of water with $Ce^{4+}$.[108] Palladium-doped $SO_3H$-functionalized ethylene-bridged HPMO NPs were found to be more efficient than bulk mesoporous silica, but lower than organically doped HMSN for the catalysis of methyl isobutyl ketone from acetone.[131]

### 3.2- PMO NPs in Nanomedicine

Another area of great interest for PMO NPs concerns biomedical applications. Once again, the nanosized of PMO is crucial for applications, since the size of nanoparticles governs their biological interactions and lifespan with parameters such as the cellular uptake, blood circulation, tumor accumulation, etc. Besides, the introduction of particular organic groups in the PMO matrix greatly modify the biodegradability of NPs. Additionally, the organic nature of the pores enables the modulation of their hydrophobicity and host–guest interactions for high loading capacities.

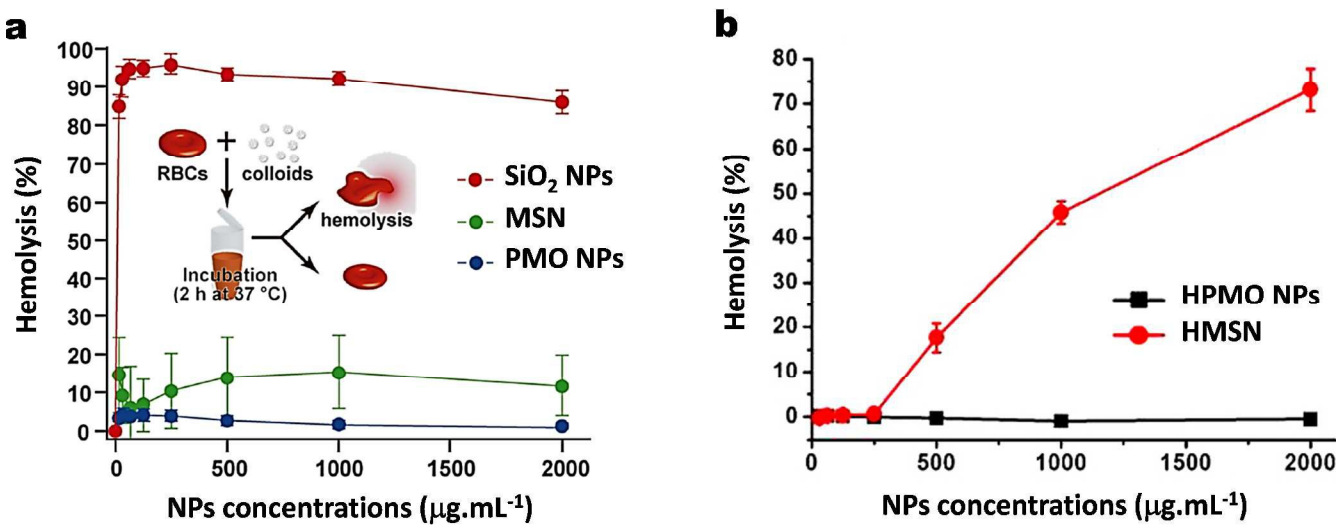


**Figure 12** Percentage of hemolysis of RBCs after incubation of silica NPs, MSN, and ethylene-bridged PMO NPs at different concentrations (a). Each data point represents the mean (standard deviation of three independent experiments). Adapted with permission, copyright 2011, American Chemical Society.[100] Percentage of hemolysis of RBCs after incubation with benzene-bridged HPMO NPs and HMSN at different concentrations (b). Adapted with permission, copyright 2013, Wiley.[3]

**Biocompatibility studies**. The interactions between this new kind of NPs and the biological media might thus drastically change compared to MSN. The first studies carried out showed that ethenylene-bridged PMO colloids were very low hemolytic materials in comparison with MSN and non-porous silica NPs (see Figure 12a). After 2 h incubation of NPs at different concentrations in PBS solution against human red blood cells (RBCs), almost no hemolytic effect was observed by the PMO NPs. This fact has been generalized for phenylene, ethylene and ethenylene HPMOs, and is related to the low amount of silanol groups present on the surface, by contrast to silica NPs (Figure 12b).[3] In fact, the hemolytic behaviour of phenylene-bridged HPMO NPs was much lower than hollow MSN (HMSN) prepared in similar conditions (Figure 12b). Furthermore, the *in-vivo* histocompatibility of HPMOs for up to two months was tested at 100 mg $kg^{-1}$ on mice with no tissue degradation or abnormal behaviour of the animals. A good biocompatibility was also shown for methylene-bridged PMO NPs with HeLa cells, with less than 25% cell death at 125 μg $mL^{-1}$.[101] These PMO NPs were easily internalized within HeLa cells, as revealed by confocal microscopy. Very recently, large pores (4.6 and 7.6 nm) PMO NPs were also found to be internalized in MCF-7 cells, of low cytotoxicity (less than 20% after 72 h of incubation), and dissolving at very slow rates (1-2 wt% in 6 days).[135] In conclusion, these first studies suggest that PMO nanomaterials can be considered as highly biocompatible thus promising for nanomedical applications, though the cytotoxicity may vary significantly for different organic bridging groups.

**Drug delivery.** Preliminary studies in 2010, showed that rhodamine B loaded ethylene-bridged HPMO NPs functionalized with pH-responsive supramolecular nanovalves enabled tunable release at pH 4 or 10 in water and or in acetonitrile.[119] The first *in-vitro* studies for the delivery of drugs were only published in 2013.[3] A payload of 14 wt% of silibinin was reached in phenylene-bridged HPMO NPs, with a reduction by 88% of the invasiveness of the highly metastatic MDA-MB-231 cells. PMO nanospheres and nanorods based on ethenylene and bis(propyl)disulfide fragments were also applied for doxorubicin (DOX) release. A high drug payload (22 wt%) could also be charged within these PMO NPs, which is twice higher than MSNs in similar conditions, thanks to specific interactions between organic fragments and drug molecules.[2] Unlike mesoporous silica, which isoelectric point is situated from 2 to 3, various PMO NPs were reported with an isoelectric point between 4.5 and 5.5,[2, 78, 136, 137] which accounts for the pH-sensitive loading and release observed in such materials.[2, 137] The endocytosis of these PMO nanospheres and nanorods was demonstrated by propidium iodide transportation within the pores of the NPs, and conversely to MSN,[138] PMO nanospheres were more uptaken than nanorods after 24 h (Figure 13g). The efficient DOX delivery via pH variation was demonstrated in MCF-7 breast cancer cells, with a cell death of 85-90% at only 1 μg.$mL^{-1}$ of NPs (Figure 13h). An important feature of

these mixed PMO NPs is the biodegradability brought by the disulfide functions. Indeed, in simulated biological media the biodegradation of the NPs was observed within 48 h: when the NPs were mixed with the intra (2 mM) and extracellular (6 µM) mercaptoethanol (ME) equivalent of the glutathione reducer, the degradation occurred as clearly showed by TEM images (Figure 13a-f).[2] In these two examples, the drug delivery was induced by an internal stimuli, *ie* the higher acidity of the lysosomes *vs* the cell culture medium. However, no external stimulus has been used until now to controllably trigger the delivery of the drugs from the PMO NPs. We will see in the two following sections that drug delivery can be combined with other therapeutic techniques to induce cell killing. Another study reported self-assembled monolayers of enantiomerically-functionalized PMO nanocontainers designed for the modification of the cell adhesion behaviour. They also performed the delivery of Hoechst 33342 via these PMO NPs as proof-of-principle for drug delivery applications.[139] Bein *et al*. reported rhodamine B-loaded fluorescent ethylene-coumarin-bridged PMO NPs coated with a lipid layer for cargo delivery in HeLa cells.[136]

**High intensity focused ultrasound (HIFU) combined medicine**. The HIFU energy is locally used in biomedical applications to heat and destroy diseased or damaged tissues, which causes ablation. Recently, DOX-loaded phenylene-bridged HPMO NPs were used for *in-vivo* HIFU-actuated drug delivery via a photothermal mechanism.[140] They demonstrated the synergistic effect of HIFU hyperthermia and HIFU-triggered drug delivery with down to 72% of tumor inhibition rate with significant tumor weight loss (mass in control: 2.34 ± 0.88 g, mass after synergistic therapy: 0.63 ± 0.24 g). Accordingly, the delivery process resulted from disruption of the hydrophobic interactions between DOX drugs and the pores of the PMO shell, but no capsule damage was observed. Besides, Paclitaxel-loaded HPMO NPs were used for efficient in-vivo HIFU-actuated imaging thanks to the contrast enhancement in ultrasonography image observed after the administration of the NPs.[141] Phenylene-bridged HPMO NPs were then described for the co-delivery of DOX and genes to fight multidrug resistance of cancer cells.[142] A power-dependant HIFU-enhanced release of DOX was also obtained with HPMO NPs designed by co-condensation of phenylene and tetrasulfide based organo-bridged alkoxysilanes.[78] The use of glutathione could also enhance the release of the drug in solution, and in-vitro and in-vivo studies showed high anti-cancer efficiencies via HIFU-combined therapy.

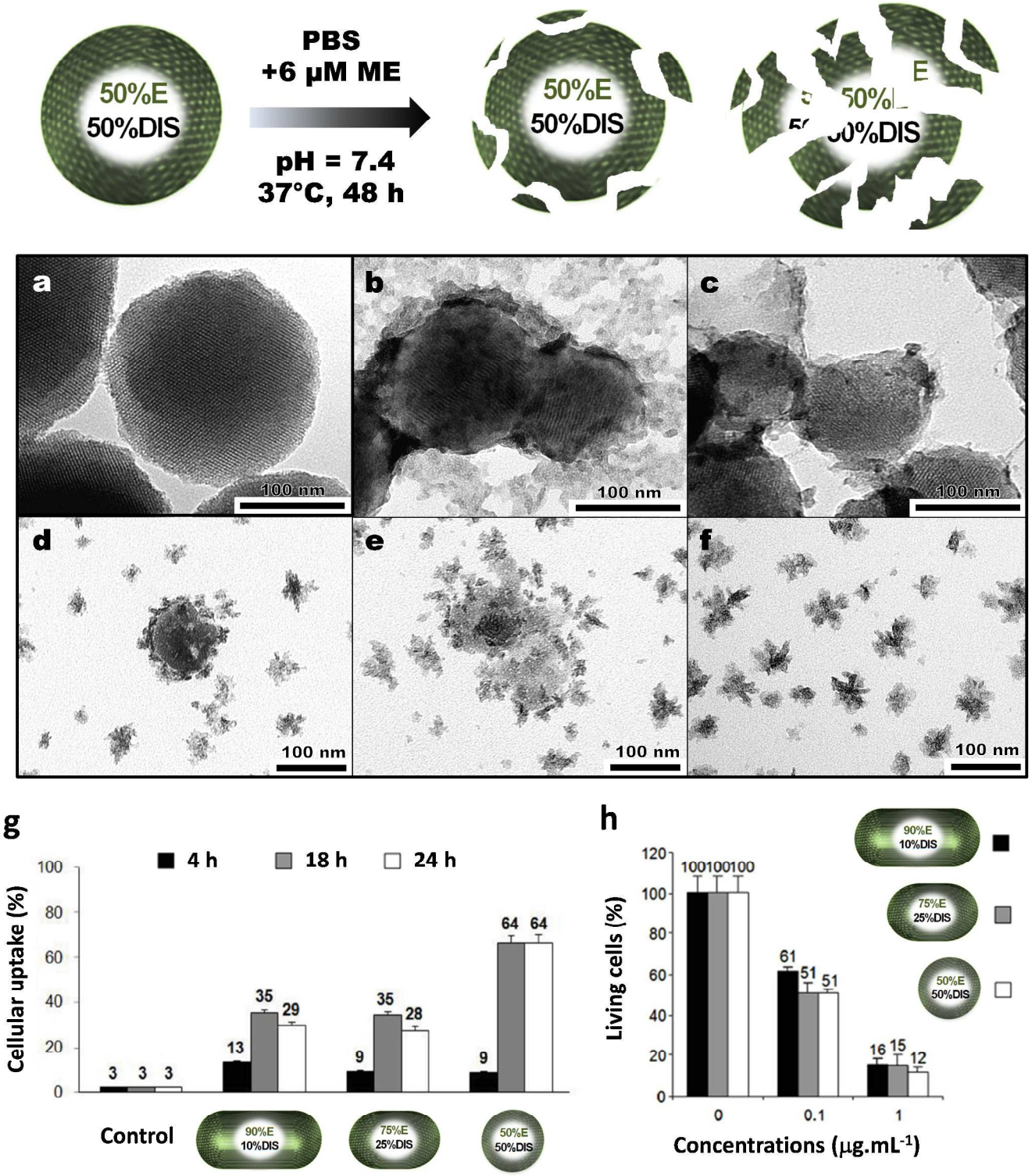


**Figure 13** TEM images of ethenylene-bis(propyl)disulfide-bridged PMO nanospheres before (a) and after 48 h of degradability control in physiological conditions (b–f). Cellular uptake quantitative analysis of ethenylene-bis(propyl)disulfide-bridged PMO nanospheres and nanorods determined via flow cytometry after 4, 18, and 24 h of incubation (g), and the in-vitro cytotoxicity studies of the DOX-loaded NPs after 72 h incubation time at various concentrations of NPs (h). Adapted with permission, copyright 2014, Wiley.[2]

**Protein Delivery**. The delivery of proteins was recently achieved by Chengzhong Yu and co-workers with large pore phenylene-bridged PMO NPs.[135] Monodisperse 50 nm spherical particles with 4.6 and 7.6 nm pores were loaded with the RNase a membrane impermeable protein (4.7 nm of hydrodynamic diameter). NPs with smaller pores were only surface-coated with proteins, while NPs composed of 7.6 nm pores adsorbed proteins on both their internal and external surfaces. Passive release profiles were obtained for both NPs in PBS at 37ºC, with a more sustained release profile with large pore PMO NPs. Nanomaterials with 7.6 nm pores were applied on MCF-7 cells and induced a significant time-dependant cell inhibition of 40, 56, and 64% after 24, 48, and 72h of incubation respectively, while free RNase A did not induce any effect. Compared with silica NPs, PMO NPs exhibited a much lower effective RNase A dosage (4 µg $mL^{-1}$) to cancer cells without the need of hydrophobic group post-functionalization to efficiently load a high amount of proteins (144.5 µg $mg^{-1}$).

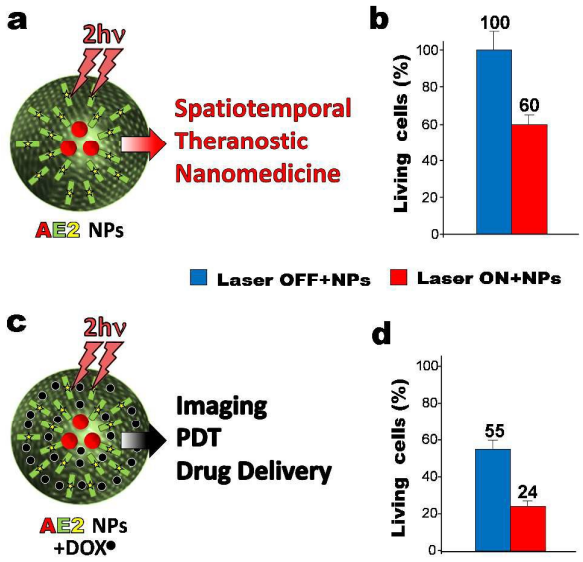


**Figure 14** Schematic representation of gold core ethenylene-2PS-bridged PMO shell NPs (a) for spatiotemporal two-photon-triggered PDT (b), and the equivalent drug-loaded NPs (c) for PDT and drug-delivery (d). Adapted with permission, copyright 2014, American Chemical Society.[143]

**Two-photon-actuated spatiotemporal medicine**. Two-photon excitation has many key advantages over conventional light irradiation for effective spatiotemporal nanomedicine such as 3-dimensional spatial resolution of the excitation at the focal point of the laser, deep and safe tissue penetration by the near-infra-red (NIR) photons, and time-controlled actuation.[40, 144-146] Hence, gold NPs embedded within an ethenylene-2PS-bridged PMO shell (AE2) NPs (see Figure 7c) were applied for two-photon-triggered theranostic nanomedicine (Figure 14a).[111, 143] Incubated in MCF-7 cancer cells, AE2 NPs were tracked in the cell interior via two-photon imaging through the plasmon-enhanced fluorescence of incorporated 2PS molecules. Upon laser irradiation in the NIR (750 nm), 40% of selective cell killing was induced with AE2 NPs via photodynamic therapy (PDT, see Figure 14b). Additionally, DOX-loaded AE2 NPs (Figure 14c) produced a synergistic cell killing through PDT and drug delivery with up to 75% of cell death (Figure 14d). A library of PMO NPs was also studied with ethenylene-, 2PS-, and phenylene-mixed bridges with or without gold core in the framework to optimize the anticancer therapy.[143] Very recently we also reported ethenylene-porphyrin-based mesoporous silsesquioxane NPs for autonomous drug delivery and NIR TPE-imaging in cancer cells.[137]

## 4- CONCLUSIONS AND ONGOING CHALLENGES

PMO nanomaterials constitute a very promising new area of research that attracts more and more scientists interested in porous materials. The unique properties available and envisioned in the pores of PMO NPs open virtually unlimited applications that will only be restrained by the imagination of the scientist and its ability to synthesis challenging novel PMO NPs with more complex frameworks. Recently, the synthesis of PMO nanomaterials has been controlled via various soft and hard templating strategies to produced PMO and HPMO NPs, nanorattles, as well as multipodal PMO NPs with small organic repetitive units (ethylene, ethenylene, phenylene). PMO NPs have been applied for various biomedical applications such as drug and protein delivery and photodynamic therapy, and have been found to be even more biocompatible than MSN. Moreover, metal core PMO shell NPs as well as post-functionalized PMO NPs have been successfully utilized for various catalytic applications.

The main challenge for the chemist is now to synthesize nanoscaled PMO with larger functional groups. We have shown that a way of incorporating larger organic groups in PMO NPs was to design so-called mixed PMO NPs, combining a small organic group to generate the porous organized framework with a larger and more functional group, specifically used in our studies for enhanced biodegradability and two-photon nanomedicine. The most interesting and challenging prospect is however to synthesize PMO NPs with 100% of larger functional groups, which can only be done if larger functional organoalkoxysilane precursors are also prepared in large quantity. The difficulty of this task lies in the

fact that large organoalkoxysilanes have unknown behaviours in a given micellar template, solvent mixture, pH, etc, and often lead to non-porous silsesquioxane bulk materials. Computational simulation may provide useful insights in that regard.[147] Nonetheless, designing novel crystal-like PMO nanomaterials based on large organic groups that could garner fascinating electronic, photonic, or mechanical properties is a sufficient motivation for the synthetic screening race that awaits chemists around the world.

## Acknowledgements

This work was supported by King Abdullah University of Science and Technology (KAUST).

## References


1. J. Croissant, X. Cattoën, M. Wong Chi Man, P. Dieudonné, C. Charnay, L. Raehm and J.-O. Durand, *Adv. Mater.*, 2015, **27**, 145–149.
2. J. Croissant, X. Cattoën, M. W. C. Man, A. Gallud, L. Raehm, P. Trens, M. Maynadier and J. O. Durand, *Adv. Mater.*, 2014, **26**, 6174–6180.
3. Y. Chen, P. Xu, H. Chen, Y. Li, W. Bu, Z. Shu, Y. Li, J. Zhang, L. Zhang, L. Pan, X. Cui, Z. Hua, J. Wang, L. Zhang and J. Shi, *Adv. Mater.*, 2013, **25**, 3100–3105.
4. N. Mizoshita, T. Tani and S. Inagaki, *Chem. Soc. Rev.*, 2011, **40**, 789–800.
5. K. Qian, F. Liu, J. Yang, X. Huang, W. Gu, S. Jambhrunkar, P. Yuan and C. Yu, *RSC Adv.*, 2013, **3**, 14466–14472.
6. T. Tani, N. Mizoshita and S. Inagaki, *J. Mater. Chem.*, 2009, **19**, 4451–4456.
7. M. Waki, N. Mizoshita, T. Tani and S. Inagaki, *Angew. Chem. Int. Ed.*, 2011, **50**, 11667–11671.
8. C. Vercaemst, M. Ide, P. V. Wiper, J. T. Jones, Y. Z. Khimyak, F. Verpoort and P. Van Der Voort, *Chem. Mater.*, 2009, **21**, 5792–5800.
9. C. Vercaemst, P. E. de Jongh, J. D. Meeldijk, B. Goderis, F. Verpoort and P. Van Der Voort, *Chem. Commun.*, 2009, 4052–4054.
10. M. Kuroki, T. Asefa, W. Whitnal, M. Kruk, C. Yoshina-Ishii, M. Jaroniec and G. A. Ozin, *J. Am. Chem. Soc.*, 2002, **124**, 13886–13895.
11. K. Landskron and G. A. Ozin, *Science*, 2004, **306**, 1529–1532.
12. J. R. Matos, M. Kruk, L. P. Mercuri, M. Jaroniec, T. Asefa, N. Coombs, G. A. Ozin, T. Kamiyama and O. Terasaki, *Chem. Mater.*, 2002, **14**, 1903–1905.
13. K. Landskron, B. D. Hatton, D. D. Perovic and G. A. Ozin, *Science*, 2003, **302**, 266–269.
14. J. Morell, G. Wolter and M. Fröba, *Chem. Mater.*, 2005, **17**, 804–808.
15. A. Keilbach, M. Döblinger, R. Köhn, H. Amenitsch and T. Bein, *Chem. Eur. J.*, 2009, **15**, 6645–6650.
16. Y. Li, A. Keilbach, M. Kienle, Y. Goto, S. Inagaki, P. Knochel and T. Bein, *J. Mater. Chem.*, 2011, **21**, 17338–17344.
17. H. Y. Wu, F. K. Shieh, H. M. Kao, Y. W. Chen, J. R. Deka, S. H. Liao and K. C. W. Wu, *Chem. Eur. J.*, 2013, **19**, 6358–6367.
18. W. Wang, S. Xie, W. Zhou and A. Sayari, *Chem. Mater.*, 2004, **16**, 1756–1762.
19. Z. Teng, X. Su, Y. Zheng, J. Zhang, Y. Liu, S. Wang, J. Wu, G. Chen, J. Wang, D. Zhao and G. Lu, *J. Am. Chem. Soc.*, 2015, **137**, 7935–7944.
20. N. Mizoshita, T. Tani, H. Shinokubo and S. Inagaki, *Angew. Chem. Int. Ed.*, 2012, **124**, 1182–1186.
21. M. Waki, N. Mizoshita, Y. Maegawa, T. Hasegawa, T. Tani, T. Shimada and S. Inagaki, *Chem. Eur. J.*, 2012, **18**, 1992–1998.
22. J. R. Deka, S. Vetrivel, H.-Y. Wu, Y.-C. Pan, C.-C. Ting, Y.-L. Tsai and H.-M. Kao, *Ultrason. Sonochem.*, 2014, **21**, 387–394.
23. M. Mandal and M. Kruk, *Z. Anorg. Allg. Chem.*, 2014, **640**, 624–631.
24. M. Mandal, A. S. Manchanda, J. Zhuang and M. Kruk, *Langmuir*, 2012, **28**, 8737–8745.
25. Y. Li, A. Keilbach, N. Mizoshita, S. Inagaki and T. Bein, *J. Mater. Chem. C*, 2014, **2**, 50–55.
26. Y. Yamamoto, H. Takeda, T. Yui, Y. Ueda, K. Koike, S. Inagaki and O. Ishitani, *Chem. Sci.*, 2014, **5**, 639–648.
27. K.-i. Yamanaka, T. Okada, Y. Goto, M. Ikai, T. Tani and S. Inagaki, *J. Phys. Chem. C*, 2013, **117**, 14865–14871.
28. N. Mizoshita, Y. Goto, Y. Maegawa, T. Tani and S. Inagaki, *Chem. Mater.*, 2010, **22**, 2548–2554.
29. N. Mizoshita, M. Ikai, T. Tani and S. Inagaki, *J. Am. Chem. Soc.*, 2009, **131**, 14225–14227.
30. S. Inagaki, O. Ohtani, Y. Goto, K. Okamoto, M. Ikai, K.–i. Yamanaka, T. Tani and T. Okada, *Angew. Chem. Int. Ed.*, 2009, **48**, 4042–4046.
31. M. Ohashi, M. Aoki, K.-i. Yamanaka, K. Nakajima, T. Ohsuna, T. Tani and S. Inagaki, *Chem. Eur. J.*, 2009, **15**, 13041–13046.
32. D. Lin, L. Hu, S. H. Tolbert, Z. Li and D. A. Loy, *J. Non-Cryst. Solids*, 2015, **419**, 6–11.
33. D. Esquivel, E. De Canck, C. Jiménez-Sanchidrián, P. Van Der Voort and F. J. Romero-Salguero, *J. Mater. Chem.*, 2011, **21**, 10990–10998.
34. D. Esquivel, C. Jiménez-Sanchidrián and F. J. Romero-Salguero, *J. Mater. Chem.*, 2011, **21**, 724–733.
35. X. Meng, T. Yokoi, D. Lu and T. Tatsumi, *Angew. Chem. Int. Ed.*, 2007, **46**, 7796–7798.
36. S. A. Trammell, B. J. Melde, D. Zabetakis, J. R. Deschamps, M. A. Dinderman, B. J. Johnson and A. W. Kusterbeck, *Sens. Actuat. B*, 2011, **155**, 737–744.
37. J. R. Deka, H.-M. Kao, S.-Y. Huang, W.-C. Chang, C.-C. Ting, P. C. Rath and C.-S. Chen, *Chem. Eur. J.*, 2014, **20**, 894–903.
38. D. Lin, L. Hu, H. You, S. H. Tolbert and D. A. Loy, *J. Non-Cryst. Solids*, 2014, **406**, 139–143.
39. S. Li, B. A. Moosa, J. G. Croissant and N. M. Khashab, *Angew. Chem. Int. Ed.*, 2015, **127**, 6908–6912.
40. J. G. Croissant, O. Mongin, V. Hugues, M. Blanchard-Desce, X. Cattoën, M. Wong Chi Man, M. Maynadier, M. Garcia, M. Gary-Bobo, L. Raehm and J.-O. Durand, *J. Mater. Chem. B*, 2015, **3**, 5182–5188
41. A. Noureddine, L. Lichon, M. Maynadier, M. Garcia, M. Gary-Bobo, J. I. Zink, M. Wong Chi Man and X. Cattoen, *Nanoscale*, 2015, **7**, 11444–11452
42. M. Gary-Bobo, Y. Mir, C. Rouxel, D. Brevet, I. Basile, M. Maynadier, O. Vaillant, O. Mongin, M. Blanchard-Desce, A. Morère, M. Garcia, J.-O. Durand and L. Raehm, *Angew. Chem. Int. Ed.*, 2011, **123**, 11627–11631.
43. Y. Fatieiev, J. Croissant, S. Alsaiari, B. A. Moosa, D. H. Anjum and N. M. Khashab, *ACS Appl. Mater. Interfaces*, 2015, 10.1021/acsami.5b07365.
44. J. G. Croissant, C. Mauriello-Jimenez, M. Maynadier, X. Cattoën, M. W. C. Man, L. Raehm, O. Mongin, M.

Blanchard-Desce, M. Garcia and M. Gary-Bobo, *Chem. Commun.*, 2015, **51**, 12324–12327.
45. Y. Fatieiev, J. Croissant, K. Julfakyan, L. Deng, D. H. Anjum, A. Gurinov and N. Khashab, *Nanoscale*, 2015, **7**, 15046–15050.
46. L. Fertier, C. Théron, C. Carcel, P. Trens and M. Wong Chi Man, *Chem. Mater.*, 2011, **23**, 2100–2106.
47. A. Chemtob, L. Ni, C. Croutxé-Barghorn and B. Boury, *Chem. Eur. J.*, 2014, **20**, 1790–1806.
48. A. Zamboulis, N. Moitra, J. J. E. Moreau, X. Cattoen and M. Wong Chi Man, *J. Mater. Chem.*, 2010, **20**, 9322–9338.
49. S. Inagaki, S. Guan, T. Ohsuna and O. Terasaki, *Nature*, 2002, **416**, 304–307.
50. S. Bracco, M. Beretta, A. Cattaneo, A. Comotti, A. Falqui, K. Zhao, C. Rogers and P. Sozzani, *Angew. Chem. Int. Ed.*, 2015, **127**, 4855–4859.
51. N. Mizoshita and S. Inagaki, *Angew. Chem. Int. Ed.*, 2015, **54**, 11999–12003.
52. C. Yoshina-Ishii, T. Asefa, N. Coombs, M. J. MacLachlan and G. A. Ozin, Chem. Commun., 1999, 2539–2540.
53. Y. Goto and S. Inagaki, Chem. Commun., 2002, 2410-2411.
54. O. Olkhovyk, S. Pikus and M. Jaroniec, J. Mater. Chem., 2005, **15**, 1517–1519.
55. O. Olkhovyk and M. Jaroniec, J. Am. Chem. Soc., 2005, **127**, 60–61.
56. V. Rebbin, R. Schmidt and M. Fröba, Angew. Chem. Int. Ed., 2006, **45**, 5210–5214.
57. C. X. C. Lin, S. Jambhrunkar, P. Yuan, C. H. C. Zhou and G. X. S. Zhao, *RSC Adv.*, 2015, **5**, 89397–89406.
58. A. S. Manchanda and M. Kruk, *Microporous Mesoporous Mater.*, 2015, 10.1016/j.micromeso.2015.10.017.
59. A. Schachtschneider, M. Wessig, M. Spitzbarth, A. Donner, C. Fischer, M. Drescher and S. Polarz, *Angew. Chem. Int. Ed.*, 2015, **127**, 10611–10615.
60. A. Carpio, D. Esquivel, L. Arce, F. J. Romero-Salguero, P. Van Der Voort, C. Jiménez-Sanchidrián and M. Válcarcel, *J. Chromatogr. A*, 2014, **1370**, 25–32.
61. F. Lin, X. Meng, M. Mertens, P. Cool and S. Van Doorslaer, *Phys. Chem. Chem. Phys.*, 2014, **16**, 22623–22631.
62. L. Grösch, Y. J. Lee, F. Hoffmann and M. Fröba, *Chem. Eur. J.*, 2015, **21**, 331–346.
63. X. Zhang, F. Su, D. Song, S. An, B. Lu and Y. Guo, *Appl. Catal. B: Environmental*, 2015, **163**, 50–62.
64. A. Finiels, B. Alonso, M. Bousmina, D. Brunel and A. El Kadib, *New J. Chem.*, 2016, 10.1039/C5NJ01824B.
65. Z. Li, J. C. Barnes, A. Bosoy, J. F. Stoddart and J. I. Zink, *Chem. Soc. Rev.*, 2012, **41**, 2590–2605.
66. P. Saint-Cricq, S. Deshayes, J. I. Zink, and A. M. Kasko, *Nanoscale*, 2015, **7**, 13168-13172.
67. S. Dib, M. Boufatit, S. Chelouaou, F. Sadi-Hassaine, J. Croissant, J. Long, L. Raehm, C. Charnay and J. O. Durand, *RSC Adv.*, 2014, **4**, 24838–24841.
68. B. Karimi, H. M. Mirzaei and A. Mobaraki, *Catal. Sci. Technol.*, 2012, **2**, 828–834.
69. B. Karimi and F. Kabiri Esfahani, *Chem. Commun.*, 2011, **47**, 10452–10454.
70. E. De Canck, I. Ascoop, A. Sayari and P. Van Der Voort, *Phys. Chem. Chem. Phys.*, 2013, **15**, 9792–9799.
71. J. Gao, X. Zhang, S. Xu, F. Tan, X. Li, Y. Zhang, Z. Qu, X. Quan and J. Liu, *Chem. Eur. J.*, 2014, **20**, 1957–1963.
72. S. Martens, R. Ortmann, F. J. Brieler, C. Pasel, Y. Joo Lee, D. Bathen and M. Fröba, *Z. Anorg. Allg. Chem.*, 2014, **640**, 632–640.
73. M. Ide, E. De Canck, I. Van Driessche, F. Lynen and P. Van Der Voort, *RSC Adv.*, 2015, **5**, 5546–5552.
74. U. Diaz, D. Brunel and A. Corma, *Chem. Soc. Rev.*, 2013, **42**, 4083–4097.
75. S. S. Park, M. Santha Moorthy and C.-S. Ha, *NPG Asia Mater.*, 2014, **6**, e96.
76. H. Takeda, Y. Goto, Y. Maegawa, T. Ohsuna, T. Tani, K. Matsumoto, T. Shimada and S. Inagaki, *Chem. Commun.*, 2009, 6032–6034.
77. M. Ikai, Y. Maegawa, Y. Goto, T. Tani and S. Inagaki, *J. Mater. Chem. A*, 2014, **2**, 11857–11865.
78. Y. Chen, Q. Meng, M. Wu, S. Wang, P. Xu, H. Chen, Y. Li, L. Zhang, L. Wang and J. Shi, *J. Am. Chem. Soc.*, 2014, **136**, 16326–16334.
79. A. Noureddine, P. Trens, G. Toquer, X. Cattoën and M. Wong Chi Man, *Langmuir*, 2014, **30**, 12297–12305.
80. I. Munaweera, J. Hong, A. D'Souza and K. J. Balkus Jr, *J. Porous Mater.*, 2014, **22**, 1–10.
81. A. Comotti, S. Bracco, P. Valsesia, M. Beretta and P. Sozzani, *Angew. Chem. Int. Ed.*, 2010, **49**, 1760–1764.
82. A. Corma, U. Díaz, M. Arrica, E. Fernández and Í. Ortega, *Angew. Chem. Int. Ed.*, 2009, **121**, 6365–6368.
83. K. Bürglová, A. Noureddine, J. Hodačová, G. Toquer, X. Cattoën and M. Wong Chi Man, *Chem. Eur. J.*, 2014, **20**, 10371–10382.
84. A. C. Gomes, M. A. Lourenço, S. M. Bruno, P. Ferreira, A. A. Valente, M. Pillinger and I. S. Gonçalves, *J. Organomet. Chem.*, 2014, **751**, 501–507.
85. S. Inagaki, S. Guan, Y. Fukushima, T. Ohsuna and O. Terasaki, *J. Am. Chem. Soc.*, 1999, **121**, 9611-9614.
86. T. Asefa, M. J. MacLachlan, N. Coombs and G. A. Ozin, *Nature*, 1999, **402**, 867–871.
87. B. J. Melde, B. T. Holland, C. F. Blanford and A. Stein, *Chem. Mater.*, 1999, **11**, 3302–3308.
88. W. Wang, J. E. Lofgreen and G. A. Ozin, *Small*, 2010, **6**, 2634–2642.
89. P. Van Der Voort, D. Esquivel, E. De Canck, F. Goethals, I. Van Driessche and F. J. Romero-Salguero, *Chem. Soc. Rev.*, 2013, **42**, 3913–3955.
90. B. Hatton, K. Landskron, W. Whitnall, D. Perovic and G. A. Ozin, *Acc. Chem. Res.*, 2005, **38**, 305–312.
91. L. Zhang, H. C. L. Abbenhuis, Q. Yang, Y.-M. Wang, P. C. M. M. Magusin, B. Mezari, R. A. Van Santen and C. Li, *Angew. Chem. Int. Ed.*, 2007, **119**, 5091–5094.
92. Y. Li, F. Auras, F. Löbermann, M. Döblinger, J. r. Schuster, L. Peter, D. Trauner and T. Bein, *J. Am. Chem. Soc.*, 2013, **135**, 18513–18519.
93. F. Auras, Y. Li, F. Löbermann, M. Döblinger, J. Schuster, L. M. Peter, D. Trauner and T. Bein, *Chem. Eur. J.*, 2014, **20**, 14971-14975.
94. H. Djojoputro, X. F. Zhou, S. Z. Qiao, L. Z. Wang, C. Z. Yu and G. Q. Lu, *J. Am. Chem. Soc.*, 2006, **128**, 6320–6321.
95. L. Zhang, S. Z. Qiao, Y. G. Jin, Z. G. Chen, H. C. Gu and G. Q. Lu, *Adv. Mater.*, 2008, **20**, 805–809.
96. C. X. C. Lin, Z. Li, S. Brumbley, L. Petrasovits, R. McQualter, C. Yu and G. Q. M. Lu, *J. Mater. Chem.*, 2011, **21**, 7565–7571.
97. S. Z. Qiao, C. X. Lin, Y. Jin, Z. Li, Z. Yan, Z. Hao, Y. Huang and G. Q. Lu, *J. Phys. Chem. C*, 2009, **113**, 8673–8682.
98. E.-B. Cho, D. Kim and M. Jaroniec, *Microporous Mesoporous Mater.*, 2009, **120**, 252–256.
99. J. Liu, S. Bai, H. Zhong, C. Li and Q. Yang, *J. Phys. Chem. C*, 2009, **114**, 953–961.

100. C. Urata, H. Yamada, R. Wakabayashi, Y. Aoyama, S. Hirosawa, S. Arai, S. Takeoka, Y. Yamauchi and K. Kuroda, *J. Am. Chem. Soc.*, 2011, **133**, 8102–8105.
101. B. Guan, Y. Cui, Z. Ren, Z.-a. Qiao, L. Wang, Y. Liu and Q. Huo, *Nanoscale*, 2012, **4**, 6588–6596.
102. E.-B. Cho, D. Kim and M. Jaroniec, *J. Phys. Chem. C*, 2008, **112**, 4897–4902.
103. P. Mohanty and K. Landskron, *Nanoscale Res. Lett.*, 2009, **4**, 169–172.
104. P. Mohanty and K. Landskron, *Nanoscale Res. Lett.*, 2009, **4**, 1524–1529.
105. M. Zhang, Y. Li, L. Bi, W. Zhuang, S. Wang, Y. Chen, B. Li and Y. Yang, *Chin. J. Chem.*, 2011, **29**, 933–941.
106. X. Liu, X. Li, Z. Guan, J. Liu, J. Zhao, Y. Yang and Q. Yang, *Chem. Commun.*, 2011, **47**, 8073–8075.
107. M. Mandal and M. Kruk, *Chem. Mater.*, 2012, **24**, 123–132.
108. X. Liu, Y. Goto, Y. Maegawa, T. Ohsuna and S. Inagaki, *APL Mater.*, 2014, **2**, 113308.
109. W. Na, Q. Wei and Z. Nie, *J. Mater. Chem.*, 2012, **22**, 9970–9974.
110. J. Croissant, D. Salles, M. Maynadier, O. Mongin, V. Hugues, M. Blanchard-Desce, X. Cattoën, M. Wong Chi Man, A. Gallud, M. Garcia, M. Gary-Bobo, L. Raehm and J.-O. Durand, *Chem. Mater.*, 2014, **26**, 7214–7220.
111. J. Croissant, M. Maynadier, O. Mongin, V. Hugues, M. Blanchard-Desce, A. Chaix, X. Cattoën, M. Wong Chi Man, A. Gallud, M. Gary-Bobo, M. Garcia, L. Raehm and J.-O. Durand, *Small*, 2015, **11**, 295–299.
112. J. Croissant and J. I. Zink, *J. Am. Chem. Soc.*, 2012, **134**, 7628–7631.
113. X. Li, L. Zhou, Y. Wei, A. M. El-Toni, F. Zhang and D. Zhao, *J. Am. Chem. Soc.*, 2014, **136**, 15086–15092.
114. S. Haffer, M. Tiemann and M. Fröba, *Chem. Eur. J.*, 2010, **16**, 10447–10452.
115. J. Liu, H. Q. Yang, F. Kleitz, Z. G. Chen, T. Yang, E. Strounina, G. Q. Lu and S. Z. Qiao, *Adv. Funct. Mater.*, 2012, **22**, 591–599.
116. N. Koike, T. Ikuno, T. Okubo and A. Shimojima, *Chem. Commun.*, 2013, **49**, 4998–5000.
117. Y. Yang, J. Liu, X. Li, X. Liu and Q. Yang, *Chem. Mater.*, 2011, **23**, 3676–3684.
118. J. Y. Shi, C. A. Wang, Z. J. Li, Q. Wang, Y. Zhang and W. Wang, *Chem. Eur. J.*, 2011, **17**, 6206–6213.
119. W. Guo, J. Wang, S.-J. Lee, F. Dong, S. S. Park and C.-S. Ha, *Chem. Eur. J.*, 2010, **16**, 8641–8646.
120. Y. Lu, H. Fan, A. Stump, T. L. Ward, T. Rieker and C. J. Brinker, *Nature*, 1999, **398**, 223–226.
121. Y. Lu, H. Fan, N. Doke, D. A. Loy, R. A. Assink, D. A. LaVan and C. J. Brinker, *J. Am. Chem. Soc.*, 2000, **122**, 5258–5261.
122. J. Gehring, D. Schleheck, M. Luka and S. Polarz, *Adv. Funct. Mater.*, 2014, **24**, 1140–1150.
123. J. Gehring, D. Schleheck, B. Trepka and S. Polarz, *ACS Appl. Mater. Interfaces*, 2015, **7**, 1021–1029.
124. A. Pauletti, G. Moskowitz, T. Millan, C. Fernández-Martín, C. Boissière, C. Gervais and F. Babonneau, *Pure Appl. Chem.*, 2009, **81**, 1449–1457.
125. S. Bai, J. Liu, J. Gao, Q. Yang and C. Li, *Microporous Mesoporous Mater.*, 2012, **151**, 474–480.
126. M. Sasidharan, K. Nakashima, N. Gunawardhana, T. Yokoi, M. Ito, M. Inoue, S.-I. Yusa, M. Yoshio and T. Tatsumi, *Nanoscale*, 2011, **3**, 4768–4773.
127. N. S. Kehr, E. A. Prasetyanto, K. Benson, B. Ergün, A. Galstyan and H. J. Galla, *Angew. Chem. Int. Ed.*, 2013, **52**, 1156–1160.
128. M. D. Esquivel Merino, E. De Canck, C. Jiménez-Sanchidrián, P. Van Der Voort and F. J. Romero-Salguero, *Curr. Org. Chem.*, 2014, **18**, 1280–1295.
129. S. S. Park, M. S. Moorthy and C.-S. Ha, *Korean J. Chem. Eng.*, 2014, **31**, 1707–1719.
130. J. Gao, J. Liu, S. Bai, P. Wang, H. Zhong, Q. Yang and C. Li, *J. Mater. Chem.*, 2009, **19**, 8580–8588.
131. P. Wang, S. Bai, J. Zhao, P. Su, Q. Yang and C. Li, *ChemSusChem*, 2012, **5**, 2390–2396.
132. H. Zou, R. Wang, X. Li, X. Wang, S. Zeng, S. Ding, L. Li, Z. Zhang and S. Qiu, *J. Mater. Chem. A*, 2014, **2**, 12403–12412.
133. Y. Yang, W. Zhang, Y. Zhang, A. Zheng, H. Sun, X. Li, S. Liu, P. Zhang and X. Zhang, *Nano Res.*, 2015, **8**, 3404–3411.
134. M. Waki, Y. Maegawa, K. Hara, Y. Goto, S. Shirai, Y. Yamada, N. Mizoshita, T. Tani, W.-J. Chun, S. Muratsugu, M. Tada, A. Fukuoka and S. Inagaki, *J. Am. Chem. Soc.*, 2014, **136**, 4003–4011.
135. Y. Yang, Y. Niu, J. Zhang, A. K. Meka, H. Zhang, C. Xu, C. X. C. Lin, M. Yu and C. Yu, *Small*, 2015, **11**, 2743–2749.
136. S. Datz, H. Engelke, C. v. Schirnding, L. Nguyen and T. Bein, *arXiv preprint arXiv:1509.02287*, 2015.
137. C. Mauriello-Jimenez, J. Croissant, M. Maynadier, X. Cattoen, M. Wong Chi Man, J. Vergnaud, V. Chaleix, V. Sol, M. Garcia, M. Gary-Bobo, L. Raehm and J.-O. Durand, *J. Mater. Chem. B*, 2015, **3**, 3681–3684.
138. H. Meng, S. Yang, Z. Li, T. Xia, J. Chen, Z. Ji, H. Zhang, X. Wang, S. Lin, C. Huang, Z. H. Zhou, J. I. Zink and A. E. Nel, *ACS Nano*, 2011, **5**, 4434–4447.
139. N. S. Kehr, H. J. Galla, K. Riehemann and H. Fuchs, *RSC Adv.*, 2015, **5**, 5704–5710.
140. X. Qian, W. Wang, W. Kong and Y. Chen, *RSC Adv.*, 2014, **4**, 17950–17958.
141. X. Qian, W. Wang, W. Kong and Y. Chen, *J. Nanomater.*, 2014, article ID 972475, 8 pages, 10.1155/2014/972475.
142. M. Wu, Y. Chen, L. Zhang, X. Li, X. Cai, Y. Du, L. Zhang and J. Shi, *J. Mater. Chem. B*, 2015, **3**, 766–775.
143. J. Croissant, D. Salles, M. Maynadier, O. Mongin, V. Hugues, M. Blanchard-Desce, X. Cattoën, M. Wong Chi Man, A. Gallud, M. Garcia, M. Gary-Bobo, L. Raehm and J.-O. Durand, *Chem. Mater.*, 2014, **26**, 7214–7220.
144. J. Croissant, M. Maynadier, A. Gallud, H. Peindy N'Dongo, J. L. Nyalosaso, G. Derrien, C. Charnay, J.-O. Durand, L. Raehm, F. Serein-Spirau, N. Cheminet, T. Jarrosson, O. Mongin, M. Blanchard-Desce, M. Gary-Bobo, M. Garcia, J. Lu, F. Tamanoi, D. Tarn, T. M. Guardado-Alvarez and J. I. Zink, *Angew. Chem. Int. Ed.*, 2013, **125**, 14058–14062.
145. J. Croissant, A. Chaix, O. Mongin, M. Wang, S. Clément, L. Raehm, J.-O. Durand, V. Hugues, M. Blanchard-Desce, M. Maynadier, A. Gallud, M. Gary-Bobo, M. Garcia, J. Lu, F. Tamanoi, D. P. Ferris, D. Tarn and J. I. Zink, *Small*, 2014, **10**, 1752–1755.
146. J. Lu, J. Croissant, J.-O. Durand, T. Guardado-Alvarez, J. I. Zink and F. Tamanoi, *Cancer Res.*, 2014, **74**, LB-9-LB-9.
147. R. Futamura, M. Jorge and J. R. B. Gomes, *Phys. Chem. Chem. Phys.*, 2013, **15**, 6166–6169.